Cement and Concrete Composites 131 (2022) 104564

Contents lists available at ScienceDirect

Cement and Concrete Composites

journal homepage: www.elsevier.com/locate/cemconcomp

Effect of highly dispersed colloidal olivine nano-silica on early age properties of ultra-high performance concrete

Y.X. Chen [a,b], S. Li [a,b,**], B. Mezari [c], E.J.M. Hensen [c], R. Yu [d], K. Schollbach [b], H.J.H. Brouwers [b,d], Qingliang Yu [a,b,*]

[a] School of Civil Engineering, Wuhan University, Wuhan, 430072, PR China
[b] Department of the Built Environment, Eindhoven University of Technology, P.O. Box 513, 5600 MB Eindhoven, the Netherlands
[c] Department of Chemical Engineering and Chemistry, Eindhoven University of Technology, P.O. Box 513, 5600 MB Eindhoven, the Netherlands
[d] State Key Laboratory of Silicate Materials for Architectures, Wuhan University of Technology, Wuhan, 430070, PR China

ARTICLE INFO

Keywords:
Colloidal silica
Ultra-high performance concrete
Olivine
NMR

ABSTRACT

Nano-silica is an important admixture for ultra-high performance concrete (UHPC). However, complex production process and agglomeration problem of conventional nano-silica significantly limit its application in UHPC. In this study, a novel highly dispersed colloidal olivine nano-silica (C-OnS) is developed. The properties of C-OnS are characterized with laser light scattering, nuclear magnetic resonance and zeta-potential. The C-OnS is applied in UHPC to enhance the cement hydration and reduce the viscosity, while a commercial sol-gel colloidal nano-silica (C-nS) is used as a reference. The effects of C-OnS and C-nS on UHPC are investigated by calorimetry, thermal gravimetry, ^{29}Si and ^{27}Al nuclear magnetic resonance, nitrogen physisorption and mercury intrusion porosimeter. The results show that the performance of UHPC is enhanced by C-OnS at early ages thanks to its higher silanol content, surface area and dispersibility. The advantages of highly dispersive, strong pozzolanic reactivity and tailorable particle size provide new possibilities for application of C-OnS in cement-based materials.

1. Introduction

Recently developed ultrahigh performance concrete (UHPC) features low water to binder ratio, large amounts of finely ground reactive powder and excessive usage of superplasticizer, showing high strength, durability and self-compacting. However, the cost and embedded energy of the produced UHPC increased significantly [1,2]. Moreover, the low w/b ratio and high usage of superplasticizer contribute to the delayed cement hydration and longer setting time of UHPC [3–7]. Therefore, the application of nano-silica in UHPC to accelerate the cement hydration at early ages is of significant interest [8–17]. However, few studies have investigated the novel type of nano-silica on the cement hydration of UHPC at very early age. Moreover, the application of nano-silica causes reduced workability and more usage of superplasticizer, in addition to its high embodied energy and the tendency to agglomerate [18,19].

In addition, although the synthesis of nano-silica is well developed and the material is widely applied in many products, for instance, tire, paint, inorganic coating, etc. [20–23], the production of nano-silica is still time-consuming and energy intensive [24,25]. For instance, pyrogenic silica (gaseous route) is produced from the silicon tetrachloride and is vaporized in a hydrogen and oxygen flame at temperatures exceeding 1000 °C (generally 1100–1800 °C) [26]. Silica precipitated with the Stöber method (wet route) is achieved by the hydrolysis and condensation of alkoxysilanes or water glass, allowing the controlled synthesis of spherical, monodisperse, nano-to micrometer-size silica [27]. However, the high-quality silica is normally produced from organic precursors using complex methods like thermal plasma or sol-gel technology, yielding nano-silica of too high purity and small quantity. Therefore, a great demand for industry is to simplify the nano-silica production and use sustainable silicate resources to apply nano silica in cement and concrete efficiently.

For the sake of increase early age performance of UHPC and improve sustainability, a recently developed novel nano-silica, produced by using waste acid and olivine, which is an abundant minerals in earth crust [28–30], can be of interest to be utilized. Specifically according to the reaction:

* Corresponding author. School of Civil Engineering, Wuhan University, Wuhan, 430072, PR China.
** Corresponding author. School of Civil Engineering, Wuhan University, Wuhan, 430072, PR China.
E-mail addresses: s.li5@tue.nl (S. Li), q.yu@bwk.tue.nl (Q. Yu).

https://doi.org/10.1016/j.cemconcomp.2022.104564
Received 25 November 2021; Received in revised form 8 March 2022; Accepted 25 April 2022
Available online 7 May 2022

$$(Mg,Fe)_2SiO_4 + 4H^+ \rightarrow Si(OH)_4 + 2(Fe,Mg)^{2+}, 223KJ/mol \quad (1)$$

The silica can be obtained by vacuum filtration and washing with distilled water. Compared to commercial nano-silica products, which are mostly produced through sol-gel method produced from organic precursor or thermal plasma using high temperature, the nano-silica can be produced from olivine in one-step process at low temperatures (50–90 °C). The previous studies [31,32] have confirmed the promising application of olivine nano silica in cement-based materials, but very few investigated the effect of the silanol content and the silicon species of olivine silica on the cement hydration of UHPC. Recent study performed by Oertel et al. [14] indicates that Stöber silica particles are by far the most reactive, followed by pyrogenic silica and the less reactive silica fume. This is mainly due to the specific surface area, surface silanol group density, total content of silanol groups and solubility in alkaline suspension. Interestingly, the olivine silica obtains an even higher silanol content of around 8-15 nm^{-2} than Stöber particles [33], while for Stöber particles, the silanol content is around 4-5 nm^{-2}. In addition, the surface area of olivine nano silica is also higher than Stöber particles. Therefore, the olivine nano-silica could have a better solubility in cement pore solution at early age than other kinds of nano-silica, thus accelerate the cement hydration at very early stage as hypothesized.

However, original olivine nano-silica may cause severe dispersion problem in cement and concrete and increase the use of superplasticizer, limits its application in UHPC. Olivine nano-silica normally exists in powder form after drying, and the secondary particle size is around 10–20 μm [29], indicating severe agglomeration. Moreover, the water demand of silica powder from olivine is very high [15]. It is also acknowledged that the nanoparticles increase the viscosity of the paste, which is especially relevant for the very low water to binder ratios required for UHPC [2,34]. Therefore, finding a way to break up the agglomerate and decrease the water demand of paste containing nano-silica is important, especially in the low w/b system.

Methods such as ultra-sonic or high shear mixing have proven to be ineffective for size reduction for high concentration nanomaterials that have high surface energy, which is the case for the olivine nano silica [28]. On the other hand, colloidal mill is best suited for samples comprised of solids immersed in a liquid suspension, which can reduce the size of suspended agglomerated nanoparticles. Several literatures [35,36] have investigated the utilization of colloidal mill to deagglomerate nano-TiO_2 particles. The results show good dispersion and reduction on the size of the nanoparticles. However, no research has investigated preparation of colloidal silica using colloidal mill. Normally, commercial colloidal silica is prepared by sol-gel method or bottom-up process, where the particles are formed by the aggregation of dissolved silica sol in the liquid state. However, the disadvantage of sol-gel technology is the low production efficiency, and the fact that these processes offer only a limited scale-up ability. Nevertheless, the top-down process allows the unlimited scale-up production of nano-silica by the comminution of coarser nano-silica particles. Therefore, the main technical novelty of this study is the creation of another way to prepare colloidal nano-silica that is promising for large scale production and sustainable. Therefore, a colloidal mill using ZrO_2 microparticles is applied in this study to prepare colloidal nano-silica from olivine, which is never reported to the best of authors knowledge. The colloidal olivine silica is further surface modified with Tween 60 to increase the stability of the silica suspension. The illustration of deagglomeration of olivine nano-silica in colloidal mill is shown in Fig. 1.

Overall, this study firstly aims to develop a method to prepare sustainable colloidal silica from olivine and break up the agglomerates using colloidal mill and then surface modified with Tween 60. Later, the as-prepared highly dispersed C-OnS is applied in UHPC to enhance the cement hydration and flowability, including rheology, early age strength, pore structure and polymerization degree of C–S–H. The mechanism of the improved performance in UHPC is explained by thermal gravimetry test (TG), ^{29}Si and ^{27}Al MAS NMR, nitrogen physisorption and mercury intrusion porosimeter (MIP). The performance of UHPC incorporating commercial sol-gel colloidal silica (C-nS) is evaluated as a comparison.

2. Experiments and methodology

2.1. Preparation of colloidal olivine nano-silica (C-OnS)

Olivine from Norway was used for the synthesis of colloidal nano-silica, which was supplied by Eurogrit (GL50). Table 1 lists the oxide composition of GL50 measured by X-ray fluorescence (XRF), together

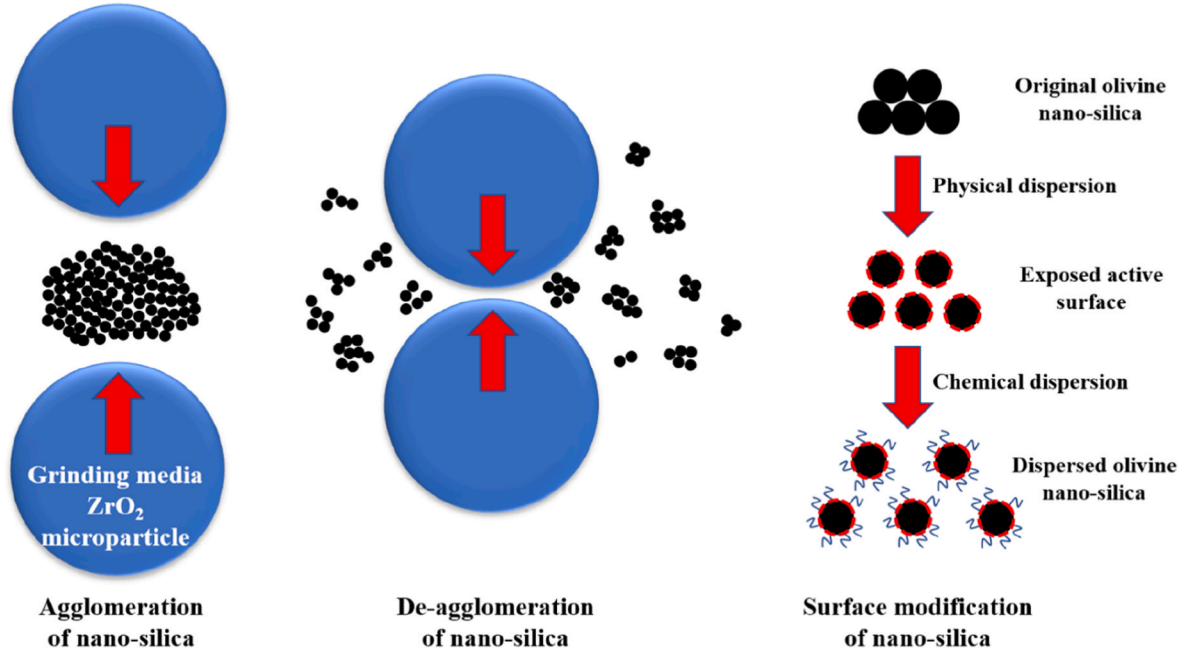

Fig. 1. Schematic illustration of deagglomeration of olivine nano-silica in a colloidal mill with grinding medias ZrO_2 microparticles and surface modified with surfactant Tween 60.

Table 1
Composition of GL-50 dunite rocks from Norway and olivine silica (wt.%) [36].

Composition	MgO	Fe_2O_3	SiO_2	Cr_2O_3	Al_2O_3	NiO	MnO	CaO	LOI[a]	Olivine
GL-50	49.3	7.32	41.4	0.31	0.46	0.32	0.09	0.15	0.59	88.9
Olivine silica	0.03	0.02	99.8	–	–	0.01	–	–	–	–

-Not detected.
[a] Loss on ignition.

with the loss on ignition (LOI) and the olivine content. Sulfuric acid was used for the acid leaching of olivine. The concentration of sulfuric acid for the silica extraction was 3 M.

Olivine nano-silica, produced by Eurosupport (the Netherlands) applying the GL-50, shows a very high purity of 99.8% as shown in Table 1. A detailed description of the process can be found in Lazaro et al. [37]. The schematic production process of two kinds of olivine nano-silica is shown in Fig. 2. The main procedure was as follows: Firstly, the olivine particles GL-50 was used to react with 3 M sulfuric acid in a thermostat reactor. Specifically, 80 g of olivine particles was dissolved in a 3 M H_2SO_4 solution at 50 °C and stirred continuously for 48 h and stirred with a mechanical stirrer constantly at 500 rpm. Afterwards, the formed mesoporous silica suspension was separated from the unreacted residues by centrifugation, followed by decantation of the lower density silica. Afterwards, the olivine silica was diluted with distilled water for filtration. The produced olivine nano-silica was then washed with a diluted H_2SO_4 solution (0.1 M) to prevent recrystallization of the sulfate salts and then washed several times with distilled water. The washed nano-silica was dried at 60 °C overnight. Lastly, the remaining water in the olivine nano-silica was removed by heating at 105 °C for 6 h. The powder olivine nano-silica (P-OnS) is ready for use. However, the agglomeration of silica is severe and the secondary particle size measured by LLS (Laser light scattering) is 17.3 μm in average as shown in Fig. 3 (a). Therefore, the deagglomeration of olivine nano-silica was performed afterwards.

For the colloidal olivine nano-silica, the filter cake of OnS after filtration was further modified with colloidal mill. A colloidal mill was used to break up the agglomerates of olivine nano-silica and further colloidization. The model of the colloidal mill was the *MiniCer* from Netsch Grinding & Dispersing system, using wet grinding and dispersing with agitator beads. The optimal procedure and processing parameters were determined by preliminary experiments and are shown as follows.

Firstly, the colloidal olivine nano-silica was prepared by mixing 200 g of silica filter cake with 20 g of demi-water using high shear mixer, and a silica suspension of 18% solid concentration can be obtained. Then, the silica suspension was further ground with the colloidal mill using two kinds of grinding media (GM), i.e. 300 μm and 100 μm ZrO_2 microparticles (Zetabeads), to prepare colloidal nano-silica with a particle size distribution d (90) lower than 1 μm. The feeding pump was hose pump (Heidolph), while the tube material was Norprene. The sealing liquid was water/glycol. The temperature during grinding was kept under 30 °C by water cooling. After the raw silica suspension was placed in the circulating tank, the colloidal mill started. The pump speed was kept at 50 rpm, while the shaft speed was kept at 3000 rpm. The stirrer tip speed was set as 9.5 m/s. The duration of the processing was kept for 120 min and afterwards the colloidal silica was ready for characterization.

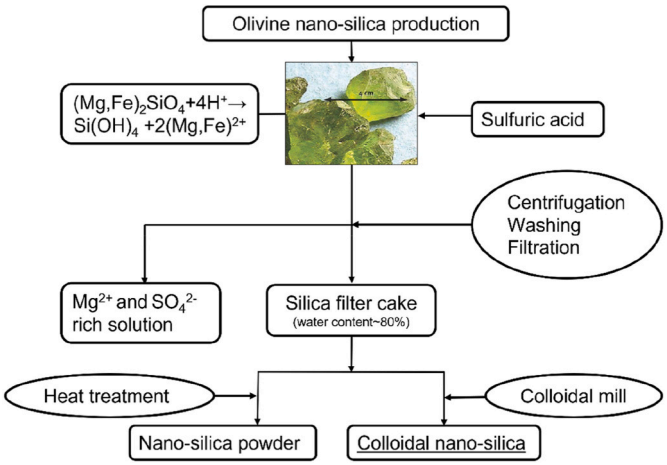

Fig. 2. The schematic process of colloidal olivine nano-silica production.

Since the suspension of the colloidal silica is unstable at neutral pH, sodium hydroxide (NaOH) was added after 60 min colloidal grinding to adjust the pH to 9, increasing the hydroxyl group (-OH) on the surface of silica for stabilization. To further stabilize the silica suspension, 0.1% Tween 60, a non-ionic surfactant was used as a surface modifier to increase the stability of C-OnS. Specifically, 1 g Tween 60 was firstly weighed and subsequently added into a 1000 g colloidal olivine nano-silica. Then, we use a vibrator to mix these two components for 2 h at room temperatures. At last, the particle size distribution and zeta potential of the modified C-OnS were measured by laser light scattering and Nano ZS.

2.2. Properties of C-OnS

2.2.1. Particle size distribution of C-OnS

The particle size distribution of the untreated olivine silica dispersion and after colloidal milling using two different grinding media is presented in Fig. 3 (a). The particle size distribution was measured with a Mastersizer 2000 linked via a Hydro S unit to disperse the colloidal silica. The used percentage of colloidal silica is below 5% due to the very small size of the silica particles. The average particle size of untreated olivine silica dispersion was around 17.3 μm. No silica particles were below 1 μm, indicating the silica agglomerated severely in the suspension. The d (10), d (50) and d (90) of the silica suspension was 7.16 μm, 18.66 μm and 48.99 μm, respectively. The PSD of colloidal silica using 300 μm and 100 μm grinding media (GM) microparticles shows different results. The PSD of colloidal silica using GM300 shows a d (50) of 558 nm, while there still exist a small shoulder at 2.45 μm, showing insufficient grinding of the silica. The d (90) of this nano-silica was 15.6 μm, showing at least 10% severely agglomerated secondary silica particles. However, the PSD of colloidal silica using GM100 shows a d (50) in the nanometer range, reaching 256 nm. It indicates the colloidal grinding using smaller grinding media (GM100) increases the efficiency of deagglomeration. Therefore, it is suggested to use 100 μm grinding media to deagglomerate the silica secondary particles.

The PSD evolution of C-OnS as a function of time, using GM100 in colloidal mill is shown in Fig. 3 (b). The percentage of silica particles with a size below 1 μm is gradually increasing with the milling time before the first 20 min, the d (50) is less than 1 μm. However, the particle size remained stable for c.a. 60 min after 20 min grinding, with 60.5% of the silica particles are in the nano-sized range. After 91 min, the particle size of silica decreased dramatically and finally 93.5% of the silica's particle size is below 1 μm after milling for 120 min. The d (90) is now less than 1 μm. Further grinding of the nano-silica has no influence on the particle size of nano-silica. The C-OnS prepared using GM100 can be defined as colloidal nano-silica and will be used for UHPC production. Fig. 4 (a) shows the TEM image of the prepared C-OnS. It is much more

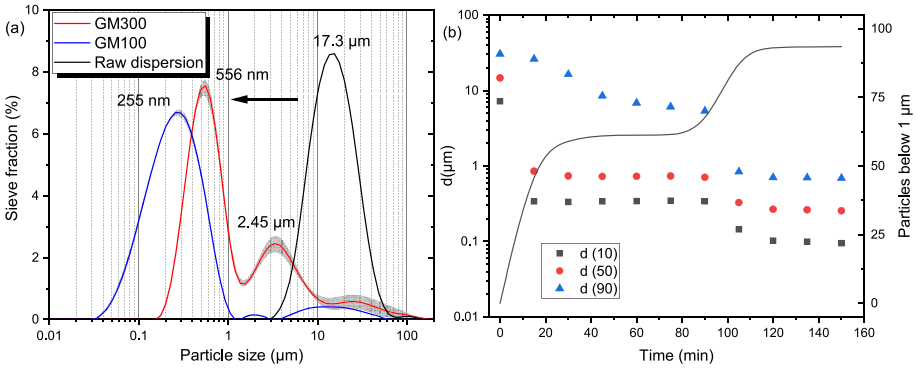

Fig. 3. (a) Particle size distribution of raw silica dispersion and treated with GM300 and GM100. **(b)** Evolution of the percentiles d (10, 50, 90) and fraction below 1 μm using GM100 with 18% solid content. The wider line shows the deviation of the particle size distribution.

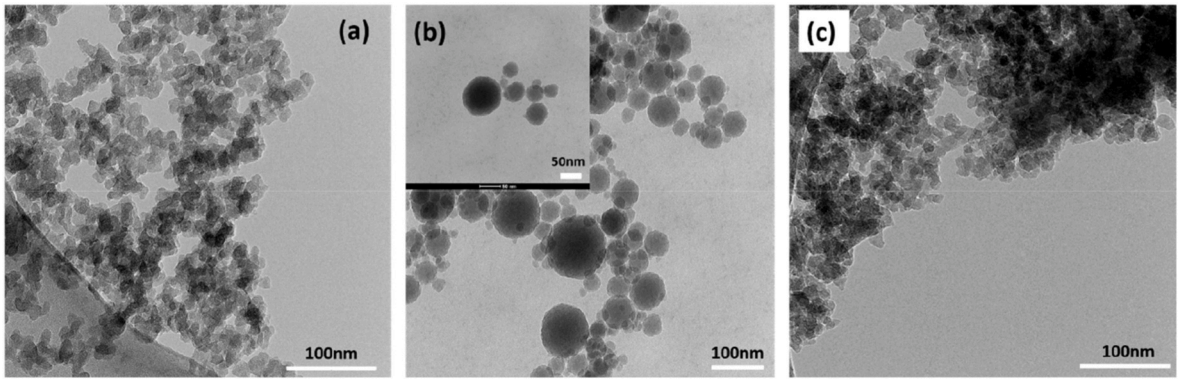

Fig. 4. TEM image of (a) C-OnS, (b) C-nS and (c) P-OnS.

dispersed than powder olivine nano-silica (P-OnS) as shown in Fig. 4 (c).

2.2.2. Zeta potential of colloidal nano-silica from olivine

The zeta potential of C-OnS with different surface treatments is presented in Table 2. The zeta potential of colloidal silica was measured with a Nano ZS from Malvern. The low zeta potential (−17.4 mV) of the original C-OnS indicates its instability and the tendency to re-agglomerate during storage. Normally, a zeta potential higher than ±30 mV is believed to create a stable colloidal suspension. Therefore, in this study, the C-OnS was kept in stable state by adding sodium hydroxide to adjust the colloidal silica pH to 9, achieving a zeta potential of −26.9 mV.

However, the absolute value of zeta potential was still less than 30 mV, indicating re-agglomeration potential (as observed after one day storage, Supplementary Information Fig. S1). Therefore, Tween 60 was added as a surface modifier in the colloidal silica to further increase the surface charge between nano-silica particles. Consequently, the zeta potential of Tween 60 modified C-OnS increased to −37.8 mV and becomes stabilized over time. The curve of zeta potential is presented in Fig. S2.

The sol-gel colloidal nano-silica (C-nS) was provided by Akzo Nobel, named Cembinder 8. The TEM image of C-nS is shown in Fig. 4 (b). The TEM analysis of olivine colloidal silica was carried out using a Tecnai 20 microscope for a microstructure analysis, operated at 200 kV. It shows the particle size has some variations from 10 nm to 150 nm. The average particle size measured from laser light scattering is around 182.3 nm. The larger particle size is due to the presence of secondary nano-silica particle. However, compared to olivine nano-silica, C-nS shows clearly round nanoparticles and less agglomeration. The solid content of C-nS was around 50%. The properties of the two kinds of colloidal silica used in this study are presented in Table 3.

2.3. Mix design of UHPC

Portland cement CEM I 52.5 R (PC), silica fume (SF), limestone powder (LP), sand 0–2 mm (S), tap water (W), and PCE-type superplasticizer (SP) were used to produce UHPC. A water/binder ratio of 0.2 was used to achieve an ultra-high compressive strength. Considering that a high content of unhydrated cement remains in UHPC, LP and SF were used to replace a certain amount of cement to decrease the usage of cement [38,39]. The chemical and physical properties of powders, i.e. PC, SF and LP, are presented in Table 4.

The TEM of silica fume used in this study can be observed in Fig. S5. As compared with original olivine nano-silica, the silica fume shows obviously less agglomeration than OnS. Although the silica fume may cause agglomeration problem during the mixing process, the surface area of silica fume is much lower (18.4 m^2/g) and used in all groups as a control concentration. Therefore, the effect of silica fume on the

Table 2
Zeta potential of colloidal silica before and after modification with sodium hydroxide and Tween 60.

Suspensions	Olivine nano-silica after colloidal grinding	Olivine nano-silica after pH adjusted to 9	Olivine nano-silica after adding Tween 60
Zeta potential (mV)	−17.4 ± 15.6	−26.9 ± 7.8	−36.0 ± 4.2

Table 3
Specification and general characteristic of the silicas.

Groups	Type	Production route	pH	Solid content (%)	BET surface area (m^2/g)	Particle size range by TEM (nm)	Average Particle size by LLD (nm)
C-OnS	Colloidal	Olivine	~9	18	300–400	10–50	163.4
C-nS	Colloidal	Sol-gel	9–10	50	50	19–156	182.3
P-OnS	Powder	Olivine	~6	99.9	300–400	10–720	17300

Table 4
Oxides composition and physical properties of raw materials.

Composition (%)	CaO	SiO_2	Al_2O_3	Fe_2O_3	K_2O	Na_2O	SO_3	MgO	TiO_2	MnO	SSA (m^2/g)	SD (g/cm^3)
PC	64.60	20.08	4.98	3.24	0.53	0.27	3.13	1.98	0.30	0.10	1.42	3.15
SF	0.90	93.06	–	2.06	1.15	0.63	1.28	0.70	–	0.07	18.4	2.32
LP	97.21	0.87	0.17	0.13	–	–	0.11	1.17	0.01	0.01	1.08	2.71

*SSA-Specific surface area; SD: Specific density.

following results is neglected. The limestone powder is also used to substitute cement, which is not a reactive powder but an inert filler in the mixture. Due to the low surface area of LP (1.08 m^2/g), the influence of LP on the flowability and viscosity is not considered in this study.

The UHPC mixture was designed based on a packing model using the Brouwers method [40,41]:

$$P(D) = \frac{D^q - D_{\min}^q}{D_{\max}^q - D_{\min}^q} \tag{2}$$

where $P(D)$ is the cumulative fractions of all particles less than size of D. D_{max} and D_{min} are the maximum particle size and minimum particle size, respectively. q is the distribution modulus, here, 0.28 was selected.

An optimization algorithm based on the Least Squares Method (LSM) was used to calculate the optimal mixture of raw materials, according to Eq. (2) [42–44]. The particle size distributions and optimal most compacted curve of the UHPC mixtures are shown in Fig. 5. The optimal design was selected as the reference recipe, following which 1% and 2% cement were replaced by C-nS or C-OnS by mass. The recipes of the UHPC mixtures are shown in Table 5.

$$RSS = \frac{\sum_{i=1}^{n}\left(P_{mix}\left(D_i^{i+1}\right) - P_{tar}\left(D_i^{i+1}\right)\right)^2}{n} \tag{3}$$

The mixing procedure of the UHPC was conducted as follows: firstly, dry mixing of all powders and sand, then, adding 75% water, which was mixed with the three kinds of silicas respectively, then superplasticizer and lastly the remaining water. After mixing, the fresh UHPC mixture was poured into molds with the dimensions of 100 × 100 × 100 mm^3 for compressive test. The molds were vibrated in a jointing table for 30s for compaction. All the samples were covered by plastic film for 24 h. After that, they were demoulded and cured in water at room temperature (20 °C) until the testing ages.

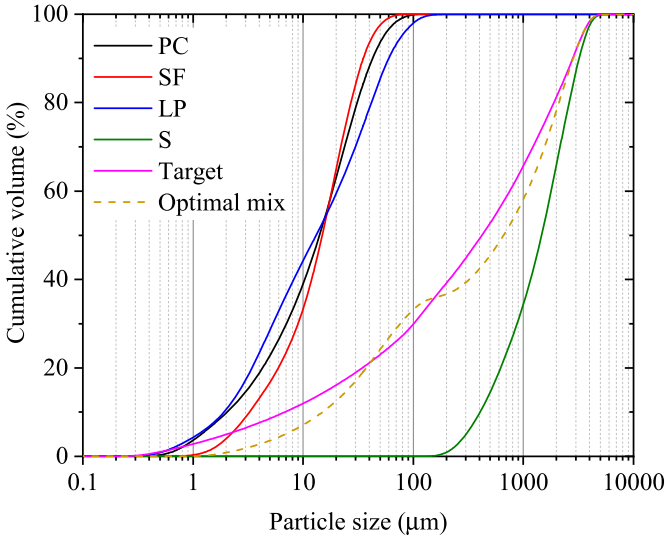

Fig. 5. Particle size distribution of raw materials.

2.4. Effect of nano-silica on UHPC

The effect of C-OnS, C-nS and P-OnS on the rheology of UHPC grout was carried out by adding C-OnS, C-nS and P-OnS in UHPC without fine aggregate. The ingredients used were Portland cement, silica fume, limestone powder, distilled water and superplasticizer. The mass ratio of the components used is shown in Table 5. The hydration products of UHPC paste and the accelerating effect of C-OnS and C-nS on the UHPC grout were determined by thermal gravimetry (TG) and calorimeter test, respectively. The chemical state of silica and alumina was studied using ^{29}Si and ^{27}Al MAS NMR. The pore structure of UHPC was evaluated by the nitrogen physisorption and mercury intrusion porosimeter (MIP).

2.4.1. Rheology test

A commercial rheometer (Anton-Paar MCR 302) with a CC27-SS (grooved) coaxial cylinder measuring geometry was used in this study. The grooved wall surface was specially designed for the cementitious system. UHPC paste was prepared by mixing portland cement, silica fume, limestone powder, water, SP and C-OnS/C-nS/P-OnS. After mixing, the UHPC paste sample was placed in the gap space of the coaxial cylinder. Then, the UHPC paste was pre-sheared at 600 s^{-1} for 1 min for the sake of breaking down the structure of the UHPC paste and rest for 3 min, creating a uniform structure before testing. The testing temperature was set at 23 ^{O}C. Later, the shear rate was set at 600 s^{-1} for 120 s, and later 500, 400, 300, 200 and 100 s^{-1} each for 60 s for the dynamic yield stress test.

Generally, UHPC paste is believed to follow a Bingham behavior, which is represented by the following equation:

$$\tau = \tau_0 + \mu_p \gamma \tag{4}$$

where τ is the shear stress, τ_0 is the yield stress, μ_p is the plastic viscosity and γ is the shear rate, respectively. The plastic viscosity was determined by calculating the slope of the shear rate versus the shear stress. The yield stress was determined by the intercept of the fitted plot of shear stress and shear rate.

2.4.2. Calorimeter test

Hydration heat was used to analyze hydration kinetics of UHPC paste with C-OnS and C-nS, which was carried out by isothermal calorimeter (TAM Air, Thermometric) using an 8-channel setup. The UHPC grout and colloidal silicas were blended with de-ionized water externally for about 3 min and vibrated with an electrical vibration mixer, then the

Table 5
Mix design of UHPC (kg/m^3).

Groups	PC (kg/m^3)	SF (kg/m^3)	LP (kg/m^3)	Sand 0–2 (kg/m^3)	SP (kg/m^3)	Water (kg/m^3)	C-OnS (kg/m^3)	C-nS (kg/m^3)	P-OnS (kg/m^3)
REF	744	42.5	170	1383	8.5	174.3	0	0	0
C-OnS 2%	729.1	42.5	170	1383	8.5	174.3	15	0	0
C-nS 2%	729.1	42.5	170	1383	8.5	174.3	0	15	0
P-OnS 2%	729.1	42.5	170	1383	8.5	174.3	0	0	15

mixed paste was injected into a sealed glass ampoule and loaded into the calorimeter. All measurements were conducted for 72 h under a constant temperature of 20 °C. The heat release and heat flow results were normalized by mass of cement.

2.4.3. Thermal gravimetric analysis

The thermal-gravimetric (TG) analysis of paste samples was conducted with a STA 449 F1 instrument. The temperature range was set from 40 °C to 1000 °C, with a heating rate of 10 °C/min in a N_2 atmosphere. The weight loss ($WL_{Ca(OH)_2}$) due to the evaporation of water can be used to calculate the amount of portlandite present, using the molecular masses of portlandite ($M_{Ca(OH)_2} = 74$ g/mol) and water ($M_{H_2O} = 18$ g/mol). The weight loss of $C_{1.5}SH_4$ due to the evaporation of water can be used to calculate the amount of C–S–H present, using the molecular masses of C–S–H with a C/S = 1.5 ($M_{C_{1.5}SH_4} = 216$ g/mol). The percentage of C–S–H and portlandite in cement paste was calculated according to:

$$Ca(OH)_2 = WL_{Ca(OH)_2} \times M_{Ca(OH)_2}/4^{*}M_{(H_2O)} \tag{5}$$

$$C_{1.5}SH_4 = WL_{CSH} \times M_{CSH}/M_{H_2O} \tag{6}$$

where $WL_{Ca(OH)_2}$ is the mass loss of water during temperature of 440–480 °C according to DSC using a tangential method. The WL_{CSH} is the mass loss of water during temperature of 105–400 °C. $M_{Ca(OH)_2}$ is the molecular mass of portlanite, M_{CSH} is the molecular mass of C–S–H using a formular of $C_{1.5}SH_4$.

2.4.4. Pore structure analysis

Nitrogen physisorption was performed with a Tristar II equipment (Micromeritics) at 77 K using liquid nitrogen to determine the specific surface area and gel pore structure of hardened UHPC paste at the age of 1, 3 and 7 day using the BET theory and the BJH theory. Before testing, the UHPC was pretreated in nitrogen gas flow at 40 °C for 4 h to remove any moisture and evaporative impurities. UHPC samples with 2% C-nS and 2% C-OnS were tested to indicate the difference. The mercury intrusion porosimetry (Micromeritics) was conducted to determine the pore size distribution of UHPC. The UHPC mortars without fine sand at the age of 7 day were crushed into small fractions (2 mm–4 mm) for MIP analysis. The intrusion pressure is from 0 to 227 MPa. The contact angle was 130.00°.

2.4.5. NMR analysis

NMR measurements were performed on a Bruker AvanceNeo 500 MHz spectrometer operating at 99 MHz and 132 MHz for ^{29}Si and ^{27}Al, respectively. The ^{29}Si MAS NMR spectra were obtained using a 4 mm CPMAS probehead and a 4 mm zirconia rotor by employing a spinning speed of 10.0 kHz. A high-power proton decoupling direct excitation (DE) pulse sequence with a 90° pulse width of 4 μs and a relaxation delay of 20 s was used. The solid-state ^{27}Al MAS NMR spectra were obtained using a 2.5 mm CPMAS probehead and a 2.5 mm zirconia rotor spinning at a speed of 25 kHz. A single pulse sequence with a 18° pulse duration of 1 μs and an interscan delay of 0.5 s was used. The ^{29}Si and ^{27}Al chemical shifts were referenced to Tetramethylsilane (TMS) and saturated Al $(NO_3)_3$ solution, respectively.

The deconvolution of the ^{29}Si MAS NMR spectra was carried out using Origin 2019, which is in accordance with the deconvolution algorithm shown in the literatures [32,45]. The multipeak fit was used to calculate the area of each peak of silicon state exists in the spectra with Gaussian function, thus the cumulative integrated percentage of each silicon in the UHPC is obtained. The mean chain length of C–S–H is calculated according to Ref. [46]:

$$MCL_{nc} = \frac{2\left[Q^1 + Q^2 + \frac{3}{2}Q^2(Al)\right]}{Q^1} \tag{7}$$

$$MCL_{c} = \frac{4\left[Q^1 + Q^2 + Q^2(Al) + Q^3 + 2Q^3(Al)\right]}{Q^1} \tag{8}$$

where MCL_{nc} is the mean chain length of non-crosslinked C-(A)-S-H structure, MCL_c is the mean chain length of crosslinked C-(A)-S-H structure, Q^n represents the silicon state of Q^1, Q^2, Q^3, while Q^n *(Al)* represents the silicon is replaced by alumina in the structure of C-(A)-S-H.

The degree of cement hydration is calculated according to:

$$\alpha = \left[100 - I\left(Q^0\right)\right] \times 100\% \tag{9}$$

where α is the hydration degree of C_3S and C_2S in the cement, $I\ (Q^0)$ is the cumulative integrated intensity percentage of Q^0.

3. Results and discussions

3.1. Rheology of UHPC paste

The shear stress and shear rate of UHPC paste before and after the addition of C-OnS, C-nS and P-OnS are shown in Fig. 6. The results show that the plastic viscosity of all the UHPC paste in this study are from 0.8 Pa•s to 1.7 Pa•s. It is observed that the reference UHPC paste without nano silica shows the lowest plastic viscosity compared to other groups, reaching only 0.8 Pa•s, which is due to the high dosage of superplasticizer. The rheology results show a trend of increased yield stress after the addition of nano-silica, regardless of it is in colloidal or powder form. However, it is observed that P-OnS leads to a much higher yield stress (400.8 Pa) than C-OnS (100.1 Pa) and C-nS (50.6 Pa). Moreover, the agglomerated P-OnS increases the plastic viscosity of the UHPC paste to a much higher degree, which is 1.7 Pa•s calculated from the slope of the fitted line in Fig. 6 (b). This is caused by the uneven distributed agglomerated silica in the UHPC paste and also the higher water demand of dry silica. Firstly, the micron sized secondary silica particles in the paste mitigate the cement particles sliding as shown in Fig. 7 (c). Secondly, the silica competes with the water that is needed for cement particles to flow, leading to higher viscosity of UHPC paste after mixing and during testing.

The colloidal silica shows less negative effect on the rheology of UHPC. The addition of C-OnS increases the plastic viscosity of the UHPC paste. However, the rising yield stress and plastic viscosity caused by C-OnS is much lower compared to P-OnS. The plastic viscosity of UHPC paste with 2% C-OnS is 1.4 Pa•s. Hence, the surface modification and colloidization of olivine silica has a positive effect on the reduction of viscosity and leads to a better performance in workability of UHPC paste. This is because the C-OnS is more dispersed in water after colloidal milling. The secondary silica particles are much smaller compared to P-OnS. This reduction in particle size of agglomerates leads to the better filling of inter-particle pores of the micron-sized particles like cement and limestone powder, thus reducing the water demand of

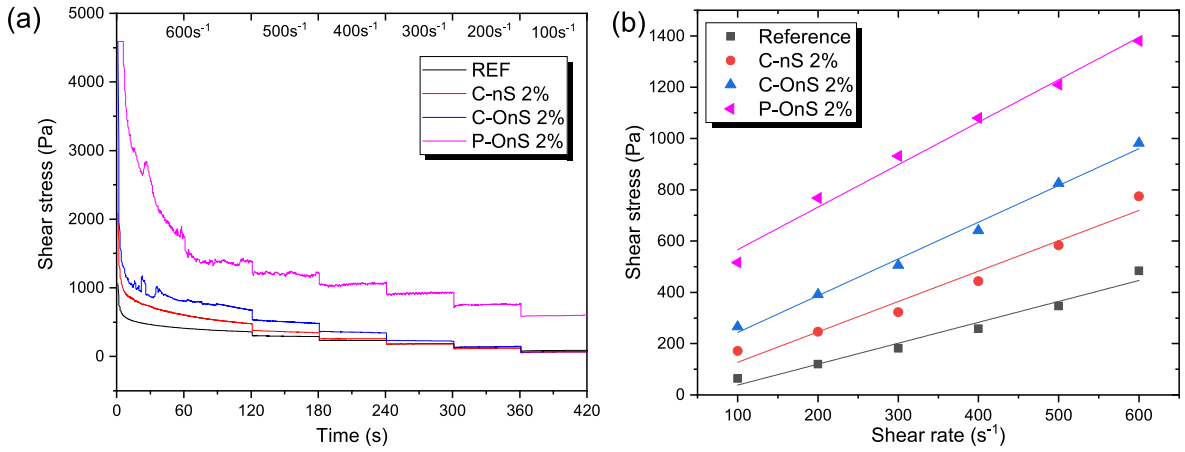

Fig. 6. Rheology result of UHPC paste with incorporation of C-nS and C-OnS: (a) Shear stress vs time (b) shear stress vs shear rate.

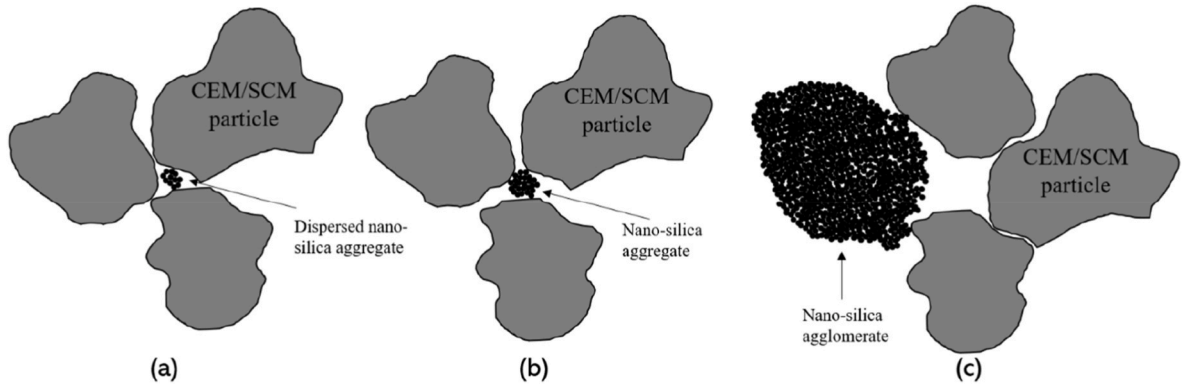

Fig. 7. Schematic illustration of dispersed nano-silica and agglomerated nano-silica impact on the packing of UHPC.

the paste. The microparticles can slide much better compared to UHPC paste containing P-OnS. The primary particle size of C-OnS is also smaller than P-OnS, thus could fill smaller nanopores and optimize the particle packing of the mixture, leading to a water reducing effect as shown in Fig. 7 (a) and (b). Thus, if the same amount of water is used for the UHPC paste, more water can be used to increase the flowability of the UHPC paste, rather than trapped inside the interparticle pores of cement and other SCMs microparticles.

The C-nS has a better performance than C-OnS in modifying the rheology. The plastic viscosity of UHPC paste with 2% C-nS is 1.2 Pa•s, which are slightly lower than the C-OnS group. This is due to the olivine silica has a rougher surface of silica particles (See TEM in Fig. 4) and higher surface area (200–300 m^2/g) than sol-gel C-nS (50 m^2/g). Hence, although C-nS and C-OnS possess the similar size of secondary particles, the microporosity and primary particle size become decisive factors in controlling the workability of paste.

Other studies demonstrated that if the PSD lowered in the nanometer range, the workability and stability could be maintained while further decreasing the necessary SP content in cementitious materials [15]. The effect of C-OnS and P-OnS on the optimum packing curve is shown in Fig. 8. The C-OnS can impact the D_{min} and then reduce the minimum boundary of PSD in the nanometer range. Furthermore, the optimized packing curve is closer to the target curve, especially from 0.1 to 10 μm, indicating a better packing of all the ingredients. This explains the reason why C-OnS has a better flowability than P-OnS. In theory, addition of nanoparticles contributes to improvement of fluidity of the UHPC paste. However, it is under the condition that nanoparticles act as inert fillers to occupy the void space among the cement and SCMs particles and thus release extra water to other parts of the paste to increase

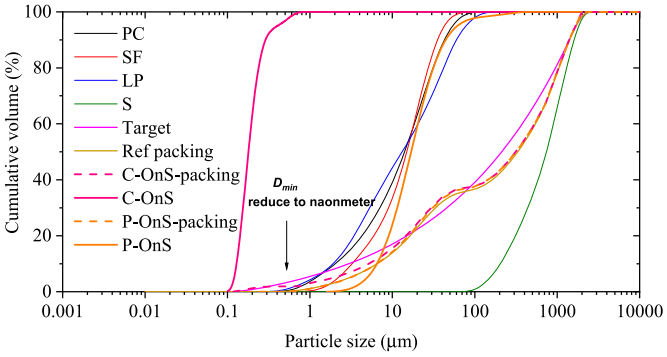

Fig. 8. Target line and composed mix using the optimization algorithm for UHPC paste with C-OnS and P-OnS.

flowability. However, the fact is nano-silica aggregate or agglomerate possesses numbers of micropores that consumes free water which help to improve flowability. Therefore, the plain UHPC paste still have the best flowability than samples containing colloidal nano-silica.

3.2. Reaction kinetics of cement paste and UHPC paste with C-OnS and C-nS

Due to the P-OnS has a significant negative influence on flowability of UHPC paste and is different from colloidal silica that pre-dispersed in water, which will lead to bias of the result, hence we choose C-OnS and C-nS to compare the effect on hydration of UHPC in the following

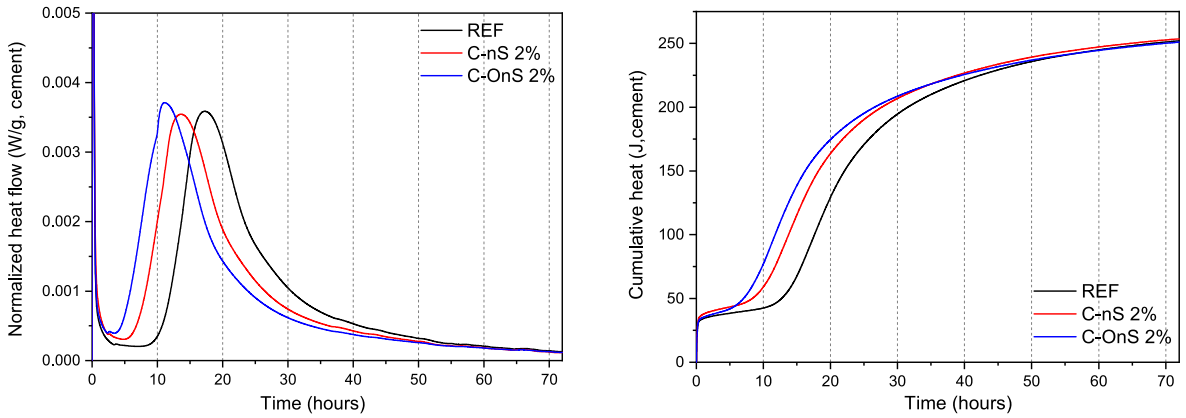

Fig. 9. Normalized heat flow and cumulative heat of UHPC grout (w/b = 0.2) with C-OnS and C-nS.

sections. The reaction kinetics of UHPC paste with addition of C-OnS and C-nS using calorimetry is shown in Fig. 9. The plain UHPC paste shows a longer time to reach the hydration peak than normal cement paste, which is due to the retardation effect of high dosage of superplasticizer and the low w/b ratio. The time to reach the hydration peak is longer (20.6 h) compared to plain cement paste with a 0.5 w/b (12 h), also the intensity of the peak is lower as shown in Fig. S3 (Supplementary information). After addition of C-nS and C-OnS, the TRP (Time to Reach Peak) reduced to 14.6 h for 2% C-nS, and 12.5 h for 2% C-OnS. It is obvious that the accelerating effect of C-OnS is stronger than that of C-nS. This phenomenon is in accordance with the results from the plain cement paste with these two kinds of nano silica as shown in Fig. S3.

The results are attributed to the different silica production process. As shown in the literatures [33,37], the olivine silica has a silanol content of 8–15 OH/nm^2, while sol-gel C-nS contains a lower silanol content of around 3–4 OH/nm^2. A higher silanol content on the surface of silica indicates a higher reactivity and compatibility with cement paste, because of the higher solubility of the silicate ions in water and the reaction with cement hydration products like portlandite is more intense.

Another reason should be the higher surface area of C-OnS compared to C-nS. The surface area of C-OnS is 200–300 m^2/g, while for C-nS is around 50 m^2/g. Therefore, the reactive surface area is much larger for C-OnS and can effectively release more silicate species and expose more reactive sites than C-nS. Another reason could be the filler or nano-seeding effect of nano-silica. However, the nano-seeding effect is not obvious from the calorimetry. It can be observed that the intensities of the hydration peaks from C-nS samples are slightly lower than those of REF and C-OnS. The lower intensity could indicate the filler effect is present during the first 24 h of hydration for C-nS, showing an accelerated TRP and less hydration heat. These results of hydration kinetics are mostly in agreement with previous researches. Oertel et al. [14] show that Stöber silica particles have a positive effect on the hydration of cement paste, however they are less stronger than pyrogenic silica, showing similar trend in this study, as the C-nS is also a Stöber particle synthesized from sol-gel method. However, the effect of C-OnS on the hydration of cement at low w/b ratio has not been previously reported. Therefore, further investigation is needed to better explain the mechanism.

3.3. Thermogravimetric analysis

The thermal gravimetric curve of the UHPC paste with addition of C-OnS and C-nS, together with the calculation of the concentration of C–S–H and portlandite in UHPC paste are shown in Fig. 10 (a) and **(b)**. The amount of C–S–H is calculated assuming a fixed composition for all samples and is only an indication for the true amount of C–S–H present. The main differences of UHPC and plain cement paste are the low w/b ratio and high usage of SP, featuring a slow hydration during the early ages. The C–S–H content in the reference UHPC paste increases with increasing aging time from 1 d to 7 d, reaching 16.1%, 22.0%, and 24.4%, respectively. On the other hand, the C-OnS groups present a higher C–S–H content in the UHPC paste. For group C-OnS 2%, the C–S–H content achieves 17.3% at 1 d and 24.5% at 3d. The commercial C-nS group shows a lower C–S–H content than those of the C-OnS series. The C-nS 2% UHPC paste has a C–S–H concentration of 16.83% at 1d and 22.4% at 3d. With the curing time reaching 7 days, the C–S–H content of C-nS 2% shows a higher content than that of C-OnS 2% (25.3%), reaching 25.7%. The results show the pozzolanic reaction happens more intense for C-nS after 7 days curing. Therefore, it can be concluded that the colloidal silica can be considered as C–S–H enhancer in the early curing for UHPC, regardless of the silica type. However, the C-OnS has a better acceleration effect than C-nS during the first 3 days, while at 7 days, C-nS presents a higher C–S–H content due to the relatively slow pozzolanic reaction with portlandite.

Another important indicator is the portlandite content in the UHPC paste. As can be observed in Fig. 10 (b), the $Ca(OH)_2$ content in REF sample is 3.27% at 1d. For the C-OnS and C-nS samples, they all show a lower $Ca(OH)_2$ content than REF group at 1d, indicating the CH formed during the early age hydration is consumed by the silica. With the curing time increasing to 3d, more CH is produced due to the further cement hydration, the CH content increases to 4.99% for REF. The C-OnS and C-nS still has a lower CH content, reaching 4.54% and 4.56% for 2% C-OnS and C-nS, respectively. The similar amount of CH for C-OnS and C-nS proves that the pozzolanic reaction of C-nS occurs mainly during the first 3 days. When the curing time prolongs to 7 days, the REF sample presents a CH content of 5.75%, while the C-OnS and C-nS groups show the CH content of 5.27% and 4.96%, respectively. The CH consumption of C-nS exceeds that of C-OnS, meaning the C-nS starts reacting more with CH in the pore solution.

It can be summarized that the C-OnS and C-nS has a different acceleration effect compared to plain UHPC sample. The interesting finding is that the C-OnS has a higher C–S–H formation and $Ca(OH)_2$ consumption than that of C-nS during the first 3 days. The reason may be the same as explained in the case of plain cement paste. The C-OnS has a more silanol content and surface area that can be exposed to become the reactive site. The reaction with portlandite becomes more intense and the $Ca(OH)_2$ concentration is much lowered at early days. While for C-nS, due to the lower solubility of silicate in the pore solution and slower reaction with the hydration product of cement, the pozzolanic effect happens later for C-nS. The findings are in agreement with the research of Lee et al. [3] who find that amorphous silica with higher surface area has a higher amount of C–S–H formation during the first 4 days curing, while with the continuation of the hydration of UHPC, the amorphous silica with lower surface area presents a higher C–S–H content at 28 days. Therefore, the C-OnS can better promote the cement hydration at

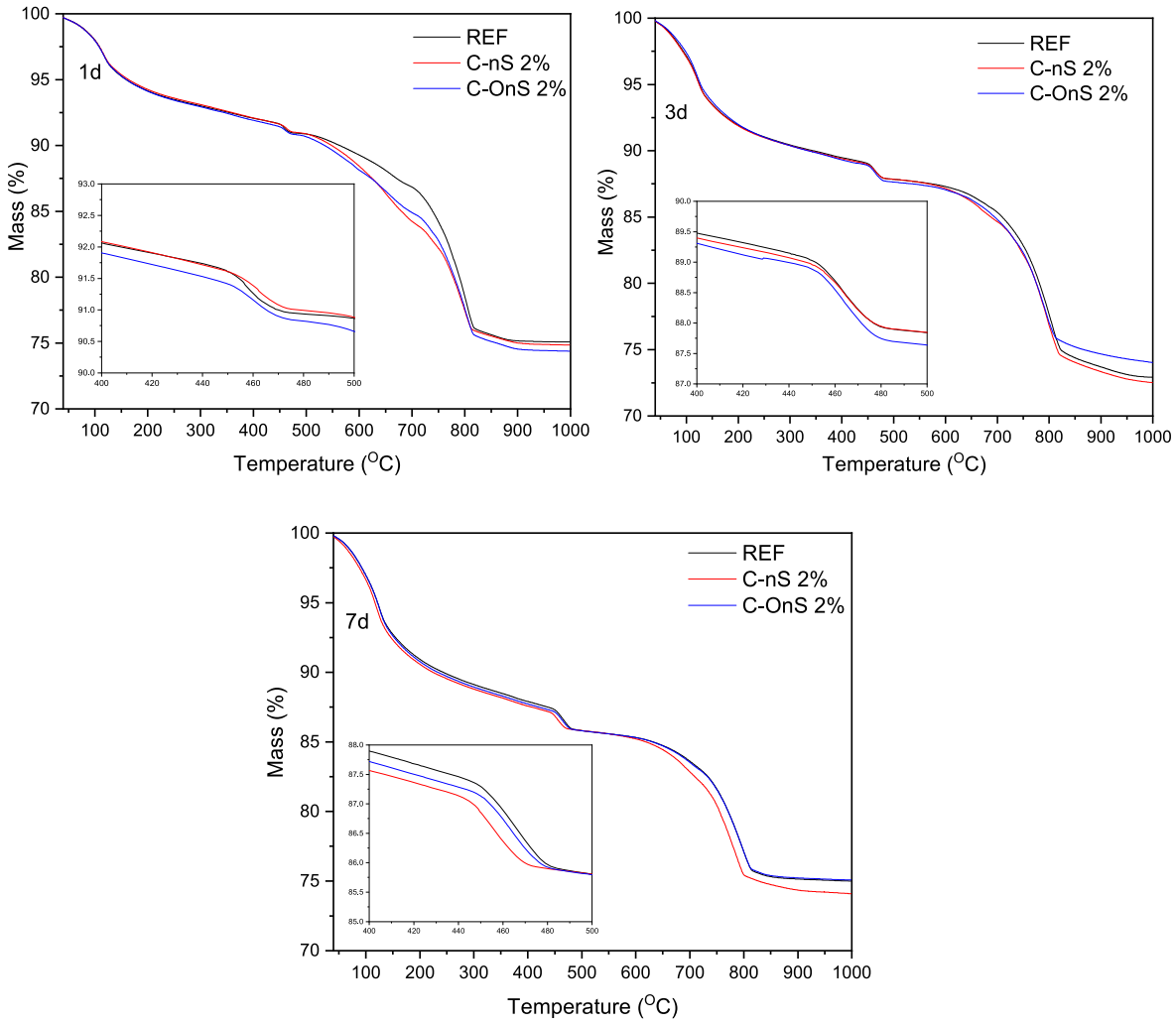

(a)

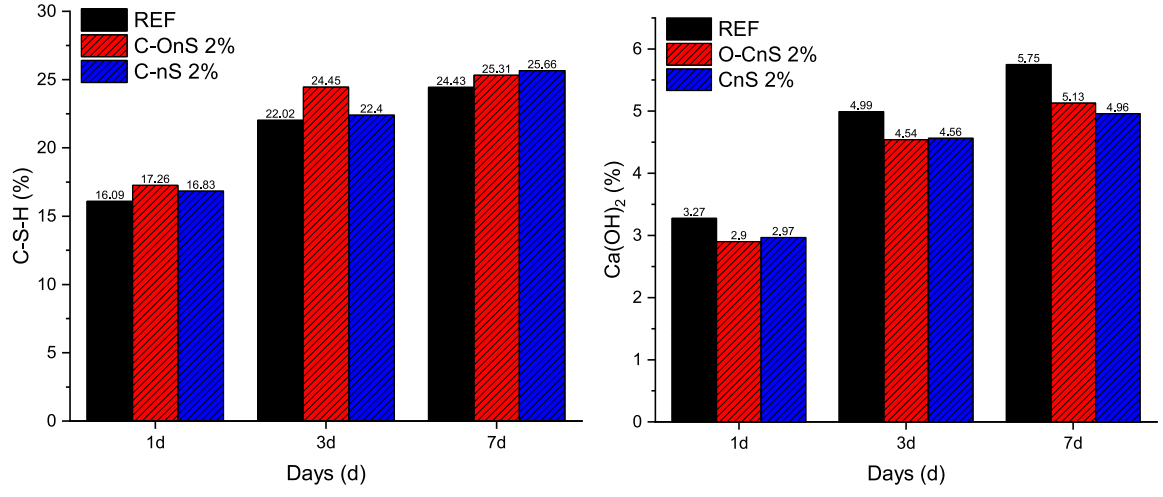

(b)

Fig. 10. (a) Thermal gravimetry analysis of UHPC paste with 2% C-OnS and C-nS at the age of 1d, 3d and 7d. (b) The C–S–H and $Ca(OH)_2$ concentration calculated from thermal gravimetry analysis of UHPC paste.

relatively early ages.

3.4. NMR analysis

3.4.1. ^{29}Si MAS NMR

The ^{29}Si MAS NMR analysis of cement, C-OnS, C-nS are shown in Fig. 11 (a). The spectra of CEM I 52.5 R shows narrow resonance and all the Si is in Q^0 state, at around −68 ppm to −75 ppm. One sharp peak at −71.4 ppm is attributed to the Belite (C_2S) phase, while the broad shoulder at −72.7 ppm is contributed by the Alite (C_3S) phase [13]. In fact, the C_3S phase has multiple resonance peaks at −69 ppm to −74 ppm contributing to the broad peak [47]. The spectra of commercial C-nS made from the sol-gel method obtains a broad peak centered at c.a. −111.3 ppm, which is a Q^4 silicate species and is similar to other silicas, for instance, pyrogenic silica or silica fume [13]. However, C-OnS made from olivine shows an additional peak at −101.5 ppm and a small shoulder at −92.1 ppm, indicating the characteristic of Q^3 and Q^2 silicate species, respectively [37]. In Fig. 11 (b), Q^3 silicate species indicates the silica surface has more isolated silanols, while Q^2 indicates the germinal silanols [48]. More Q^3 or Q^2 silicate species means a better solubility of olivine silica in cement pore solution, which may further lead to different pozzolanic reaction in the UHPC.

The plain UHPC paste hydrated at early age from 1d to 7d are mostly Q^0, Q^1 and Q^2 silicate species as shown in Fig. 12 (a). Due to the slow hydration of cement in low w/b ratios in UHPC systems, the peak of Q^0 silicate is the highest at −71.4 ppm. While for other silicate species, the intense bands at −79.4 ppm and −84 ppm are the characteristic peak of Q^1 (chain-end), Q^2_b (bridging) or Q^2_p (pair) site of C–S–H, respectively [46]. There exists another tiny shoulder at −81 ppm, attributed to the Q^2 (1Al) site, where Al species replace Si in the bridging site of C–S–H forming C-(A)-S-H [49]. The resonance at −89 ppm and −94 ppm are attributed to the Q^3 (1Al) site and Q^3 site, which are observed with very low intensity. This is due to the slow cement hydration of UHPC forming short non-crosslinked C–S–H chains, with a relatively low polymerization degree. Therefore, the mean chain length (non-crosslinking) of C–S–H in REF sample only reaches 3.19 as presented in Table 6. Hence, it is suggested that the addition of the olivine nano-silica with a higher pozzolanic activity can reduce the Ca/Si ratio of C–S–H in UHPC, improving the substitution ratio of Si by Al in C–S–H and increasing the mean chain length of C-(A)-S-H, which is consistent with previous observations [13,50].

The ^{29}Si NMR of UHPC paste with the addition of C-OnS and C-nS at the age of 1d in Fig. 12 (a) showed similar resonance at −71.4 ppm and −79.1 ppm, attributed to the unhydrated cement Q^0 and C–S–H silicate species Q^1. The almost complete lack of a resonance signal at −111.3 ppm indicates that the majority of the C-OnS was consumed in the hydration process of cement within 1 day. While for C-nS, there still exist a tiny peak at the Q^4 site (1.3%), indicating that most of the silica has still not reacted in the pore solution. Therefore, C-OnS can react more rapidly with the hydroxyl group in the pore solution of UHPC and quickly form low Ca/Si ratio C–S–H (α). This is owing to the high specific surface area and the very small particle size of the C-OnS, around 10 nm compared to 50 nm for C-nS. The peak of Q^2 silicate species (−84 ppm) of C-OnS 2% at 1d is higher than that of C-nS group and REF group, indicating olivine silica forming more secondary hydration product C–S–H (α). It is calculated that the non-crosslinking MCL of C-OnS-2% is 4.43, which is longer than that of C-nS-2% (4.28), showing that C-OnS causes a stronger polymerization degree of C–S–H. While the MCL was the lowest for plain UHPC paste, reaching only 3.19. This can also be indicated by the lower hydration degree of cement as presented in Table 6.

At the age of 3 days, the peaks at −84 ppm and −81 ppm associated with Q^2 and Q^2 (1Al) sites of the C-nS-2% and C-OnS-2% continue to increase and are much higher than that of REF. The resonance signal at −111.3 ppm of Q^4 in the C-nS sample decreases to 0.6%, indicating most of the silica reacted to C–S–H (α). The MCL of the C–S–H forms in C-OnS and C-nS groups are almost the same, reaching 3.86 and 3.61, respectively. The hydration degree of cement is also accelerated at the age of 3 days for C-OnS and C-nS group, which is observed from the lower intensity of Q^0 sites compared to the reference UHPC sample, suggesting more Q^0 of silicate of the colloidal silica group is transformed to Q^1 or Q^2. The cement hydration degree reaches 46.3% and 39.7%, respectively. On the other hand, the intensity of Q^2 and Q^2 (1Al) sites of REF are still much lower than for the UHPC with colloidal silicas. Therefore, the plain UHPC normally forms C–S–H (β/γ) with a low MCL. However, there is no evidence that low MCL means lower mechanical performance of C–S–H.

Fig. 12 (d) shows the ^{29}Si NMR spectra of UHPC paste with addition of C-OnS and C-nS at 7 days. The intensity of the Q^1 peak in the C-nS 2% sample is much higher compared to that of the 3 day aged samples, indicating a higher hydration degree of cement. It surpasses that of C-OnS. This is owing to the further reaction of the remaining C-nS and hydration of C_3S or C_2S over the course of 3d to 7d. However, the percentage of Q^2 site is lower compared to 3 day according to the deconvolution calculation from Table 6, meaning more C–S–H (β/γ) is generated from C_3S and the percentage of C–S–H (α) is thus reduced. This phenomenon happens for C-OnS as well. Also, the MCL decreases for C-OnS and C-nS samples. This is owing to the fact that the main source for C–S–H is from clinker rather than nano-silica with increasing aging time. For the reference UHPC, the Q^2 peak is still very weak, therefore, the lack of colloidal silica means the main calcium silicate product is C–S–H (β/γ) rather than C–S–H (α). The correlation of increased MCL with high pozzolanic reaction in the C-OnS-2% sample is in accordance with other results [13], demonstrating that the C–S–H of

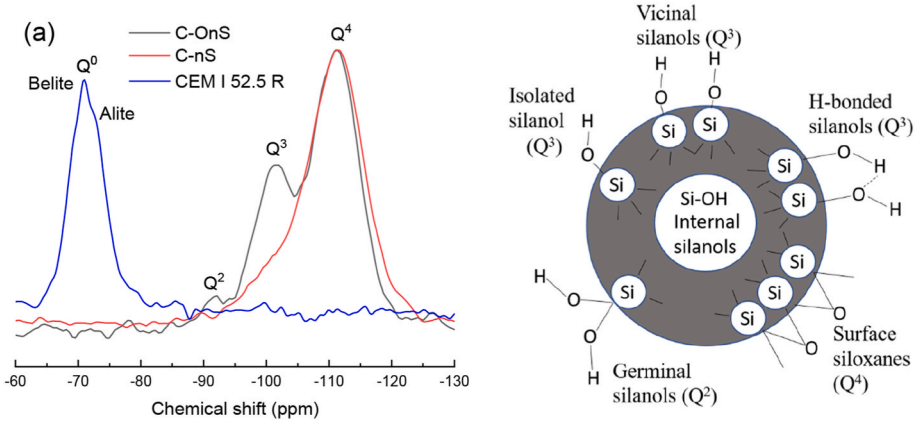

Fig. 11. (a) ^{29}Si NMR analysis of raw materials and (b) Types of silanol groups of amorphous silica: Q^4-surface siloxanes; Q^3-isolated/H-bonded/vicinal silanols; Q^2-germinal silanols.

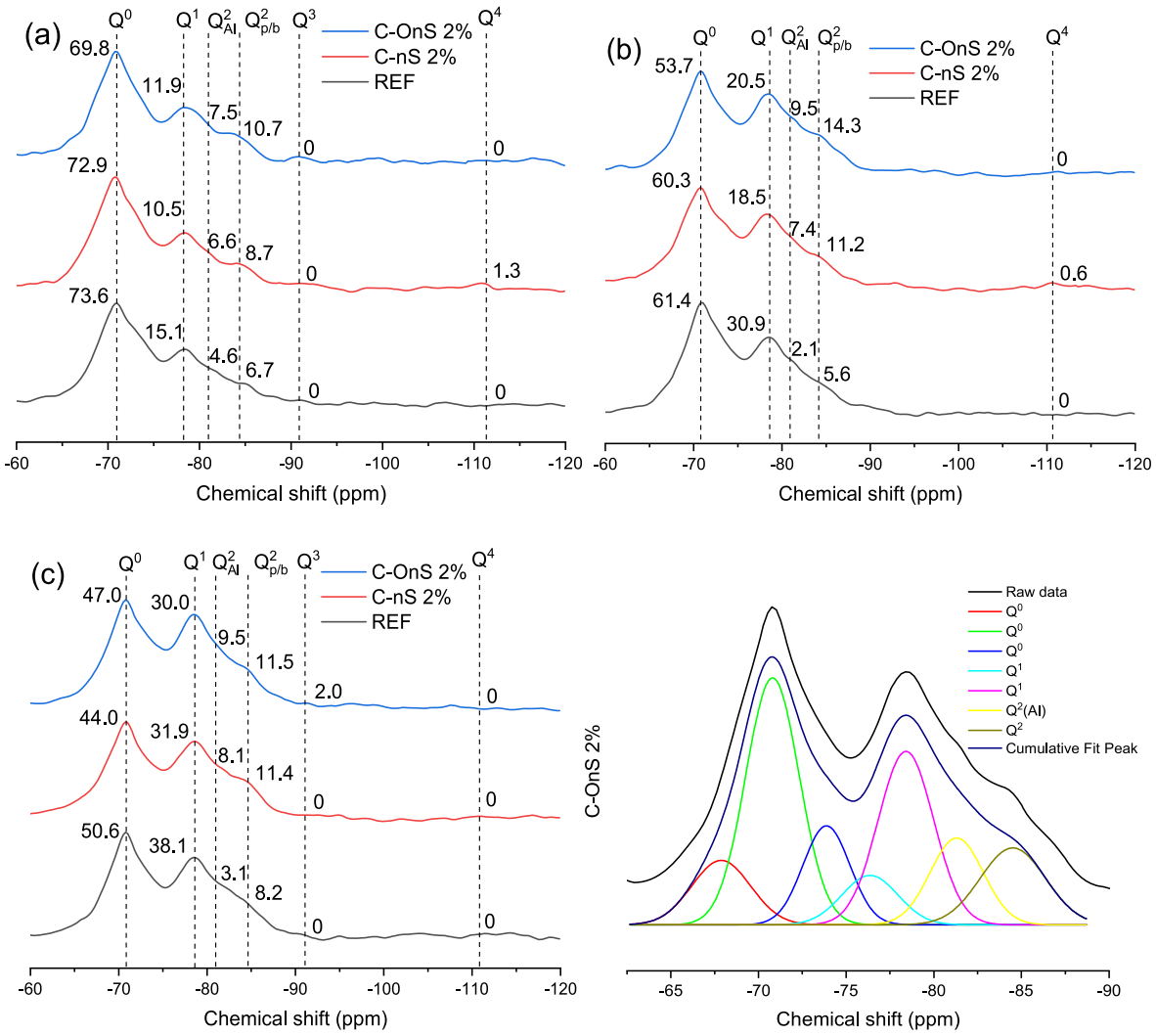

Fig. 12. ^{29}Si NMR analysis of UHPC paste at the age of (a) 1d, (b) 3d, (c) 7d and (d) example of multipeak fit for C-OnS 2% 7d.

Table 6
Mean chain length of C-(A)-S-H and hydration degree of cement in UHPC.

Groups	MCL_{nc}	Hydration degree of C_3S and C_2S in cement (%)
REF-1d	3.19	26.4
C-nS 2%-1d	4.28	27.1
C-OnS 2%-1d	4.43	30.2
REF-3d	2.43	38.6
C-nS 2%-3d	3.61	39.7
C-OnS 2%-3d	3.86	46.3
REF-7d	2.51	49.4
C-nS 2%-7d	2.97	56.0
C-OnS 2%-7d	3.08	53.0

UHPC blended with micro silica have a longer MCL than plain UHPC.

Overall, the UHPC paste with a very low w/b ratio and cured at room temperature shows a relatively slow hydration at early ages, forming quite short C-(A)-S-H chain. Compared to other literature, the transformation of Q^0 to Q^1 and Q^2 in this study is much slower, because no high temperature curing is used during UHPC preparation. However, it is clear that more C–S–H (α) is formed during the first 7 days for the samples containing silica. Hence, it can be concluded that C-OnS has a more positive effect by increasing the polymerization degree of C–S–H for UHPC paste during the first 3 days. While C-nS could have a better effect on cement hydration during 3d to 7d.

3.4.2. *^{27}Al MAS NMR*

Fig. 13 (a) presents the ^{27}Al NMR spectra of anhydrous cement 52.5 R. The broad peak situated at around 81 ppm is attributed to four-coordinated aluminum from C_3A phases [50]. The small sharp peak at 12.5 ppm is due to a small amount of cement hydration during storage forming trace amounts of AFt [51]. Fig. 13 (b) presents the ^{27}Al NMR spectra of UHPC paste at 1 day, showing a sharp peak at 12.5 ppm and a broad peak at 68.0 ppm, corresponding to Al (VI) in AFt and Al (IV) in C-(A)-S-H [46]. The small shoulder at 5 ppm is attributed to the amorphous aluminate hydrates ($Al(OH)_3$) [52]. It can be seen that the REF has the highest AFt peak while the silica containing samples show lower intensities. It can be inferred that the part of the Al species in cement that normally forms AFt is incorporated into C–S–H, thus lowering the ettringite peak. The enlarged picture showing the peak at 68 ppm is higher for C-OnS, indicating the C-OnS is already reacting at 1d. The high pozzolanic activity of C-OnS leads to a relatively low Ca/Si ratio of C–S–H (α), and thus the level of Al substitution for Si in C–S–H is increased.

With the curing time increasing to 3 days, the peaks at 68 ppm become similar for the two silica groups, but higher than the REF as shown in Fig. 13 (c). It means the C-(A)-S-H in the two silicas containing samples formed similar amounts of secondary reaction products. Al (IV) tends to substitute the Si and be octahedral-coordinated in C-(A)-S-H at a low Ca/Si ratio. The positive correlation between Al substitution for Si and lower Ca/Si ratio of C–S–H was also indicated in the ^{27}Al NMR

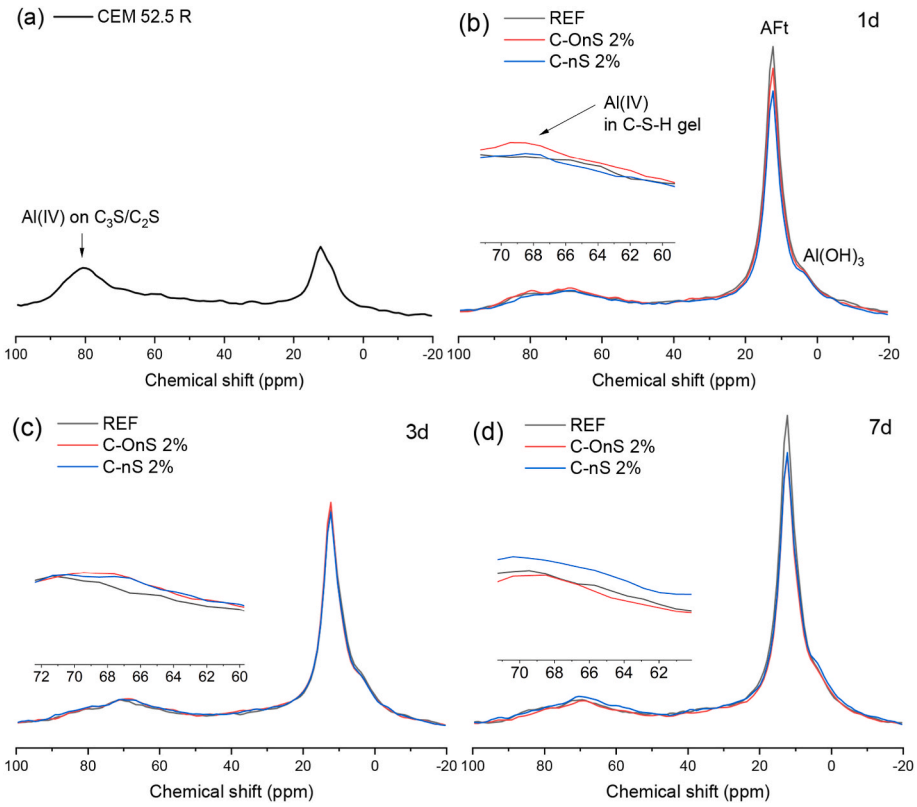

Fig. 13. ^{27}Al NMR analysis of (a) CEM 52.5 R and UHPC paste at the age of (b) 1d, (c) 3d and (d) 7d.

results from previous studies [54,55]. With the curing time reaching 7 days, the typical peak for Al (IV) in C-(A)-S-H at 68 ppm becomes higher for the C-nS containing sample, while that corresponding to Al (VI) in AFm and TAH is also higher in C-nS. This is attributed to the pozzolanic reaction happens at later ages for C-nS. While the C-OnS facilitates the pozzolanic effect at very early ages. Compared to other studies, it was also suggested that Al mostly tends to be octahedral-coordinated (i.e., AFm, AFt, and TAH) when the Ca/Si ratio of C–S–H is higher than around 1.1, while it is likely to end up with tetrahedral coordination in C-A-S-H at a lower Ca/Si ratio [56].

In summary, based on the ^{29}Si and ^{27}Al MAS NMR results, the addition of C-OnS and C-nS contributes to the Al substitution for Si in the bridging chains of C-(A)-S-H and also increases the chain length and polymerization degree of C-(A)-S-H as shown in Table 6. However, significant difference is observed in terms of the speed of pozzolanic effect occurs for C-OnS and C-nS.

3.5. Pore structure analysis

The pores in cement paste can be classified into different categories, which are (1) gel pores from 2 to 5 nm, result from internal porosity of hydration products like C–S–H gel; (2) small capillary pores from 5 to 50 nm, mainly attributed from the water amount and reaction products; (3) large capillary pores from 50 nm to 10 μm, related to the evaporable bulk water; (4) macropores larger than 10 μm, corresponding to the initial defects and air voids.

Table 7
BET surface area of UHPC paste with addition of C-OnS and C-nS.

Sample	1d (m^2/g)	3d (m^2/g)	7d (m^2/g)
REF	4.73	2.66	2.39
C-OnS 2%	7.26	5.33	5.06
C-nS 2%	6.99	4.79	4.08

The surface area and pore structure analysis of UHPC paste containing silica was performed by N_2 physisorption using BET and BJH theory, respectively. It can be seen from Table 7 that UHPC mixtures show different surface areas at different ages and different silica additions. The addition of C-OnS and C-nS increases the BET surface area of UHPC compared with the plain UHPC at 1, 3, and 7 days. The plain UHPC paste has the lowest surface area of around 4.73 m^2/g at 1 day. C-OnS 2% UHPC paste presents the highest surface area of around 7.26 m^2/g, while the surface area of C-nS 2% UHPC paste is 6.99 m^2/g. The increase in surface area is mainly due to higher amounts of C–S–H (α) formed with a low Ca/Si ratio (0.7–1.0). In addition, significant decrease in surface area is observed when the curing time is prolonged to 3 and 7 days. This is due to the higher amount of hydration products formed, mainly C–S–H and CH that create a much denser microstructure during the early hydration of cement.

The normalized and cumulative pore volume of UHPC paste with the addition of silica using the BJH method are shown in Fig. 14. The gel pore volume (2–5 nm) of the UHPC increases with the addition of silica. It can be observed that UHPC pastes with addition of these two silicas show higher gel pore volume (2–5 nm) than the plain UHPC paste from the desorption branch at 1d, which is in gel pore range. When the curing time increases to 7 days, the samples containing C-OnS still shows a higher gel pore volume than the C-nS and REF samples. Combined with the results of BET surface area, it can be suggested that the samples containing nano-silica show higher gel pore volume, which is related to the C–S–H (α) from pozzolanic reaction. On the other hand, the small capillary pores show opposite trend. The samples containing silicas have lower pore volume from 5 to 50 nm than plain UHPC sample, indicating the pore refinement by the early pozzolanic reactions.

It can also be found that the cumulative pore volume decreased for all samples with increasing time of aging from 1d to 7d. This result is in agreement with the BET surface area and can be attributed to the denser microstructure from the outer hydration products of cement particles. While it is noteworthy that the total pore volume becomes the lowest for

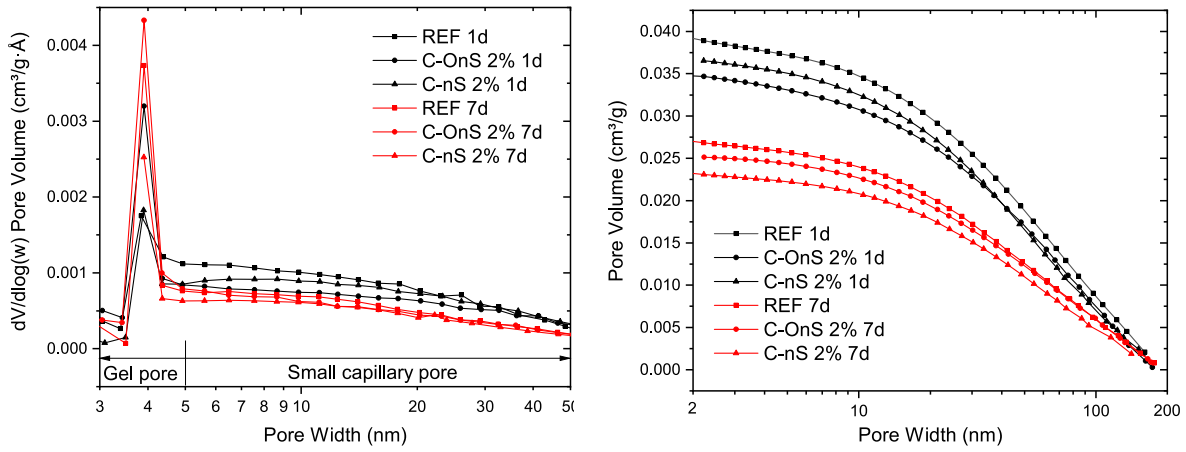

Fig. 14. The normalized and cumulative pore volume of UHPC with addition of 2% C-OnS and C-nS at 1d and 7d.

C-nS from 2 to 200 nm at 7 days. Therefore, it indicates the addition of C-nS is more effective in refining the pore structure of the small capillary pores at later ages. Meanwhile, the effect of C-OnS on the optimization of small capillary pores is limited, indicating a limited filler effect for this type of nano-silica at later ages.

The pore size distribution and cumulative pore volume of the UHPC samples at 7 day measured by MIP is shown in Fig. 15. From Fig. 15 (a), it can be observed the difference between MIP and BJH method, which shows different critical pore size due to different media used. The critical pore diameter of UHPC is from 10 to 20 nm obtained in MIP, falling in the range of small capillary pores. The intensity of the peak slightly decreases for the two silica groups. Combined with the cumulative pore volume result shown in Fig. 15 (b), it indicates the early pozzolanic effect of C-OnS and C-nS on the refinement of pore structure, and a reduction on the capillary pores could be achieved. The gel pores for C-OnS and C-nS groups is higher than that of plain UHPC paste during the first 7 days from BJH and MIP method, indicating more C–S–H gel is formed.

The cumulative pore volume versus the pore size shows a very dense pore structure for UHPC paste as shown in Fig. 15 (b). The large capillary pores and macro-pores are very limited and only account for less than 2% of the total pore volume. Most of the pore volume is accumulated from 100 nm and increases fast, and reaches the critical pore diameter at 12–14 nm, which belongs to the small capillary pore region. It is obvious that less small capillary pores are located in this region for C-nS groups. Hence another finding is C-nS can reduce the small capillary pores better than C-OnS and have more gel pores than that of C-nS. It means C-nS has a slight better effect on the optimization of the microstructure and facilitates the filler effect.

3.6. Strength of UHPC with addition of colloidal silicas

The compressive strength of the UHPC is shown in Fig. 16. All the groups show a compressive strength higher than 150 MPa at 28 days,

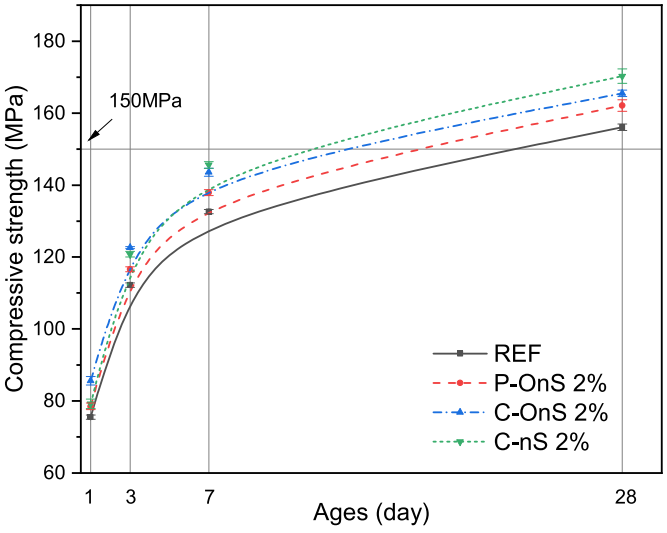

Fig. 16. Compressive strength of UHPC with silicas.

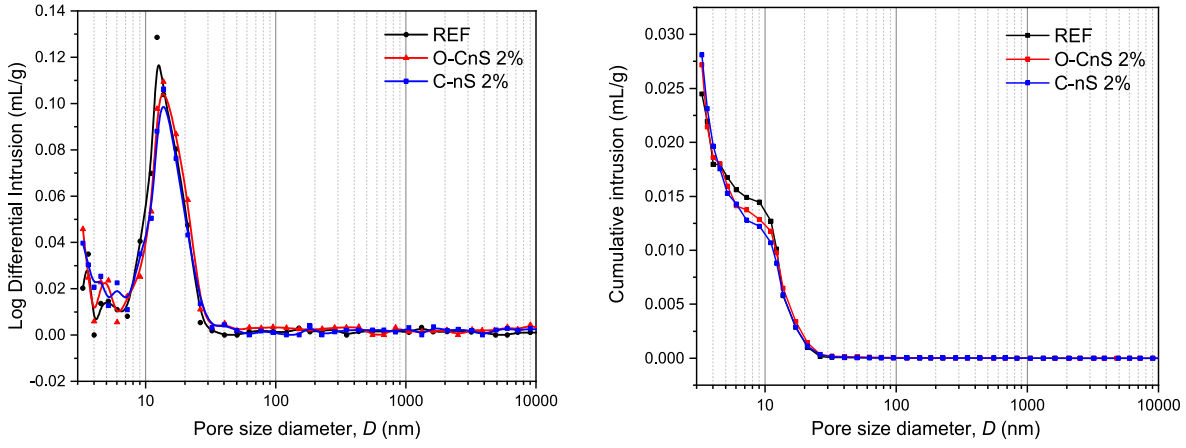

Fig. 15. The differential intrusion (a) and cumulative (b) pore volume of UHPC paste incorporated with C-OnS and C-nS at the age of 7 day.

hence reaching the requirement of UHPC [53]. The compressive strength of UHPCs during the first 7 days show a good correlation with the dosage of nano-silica. The reference group shows a strength of 75.5 MPa at 1 day while for the C-OnS and C-nS groups, the compressive strength increases to 89.6 and 79.2 MPa, respectively. However, the P-OnS group shows a very slight increase of strength compared to C-OnS. This is due to P-OnS was added in powder form. The P-OnS has particles which are agglomerated in a 3D network. This agglomerated state prevents the mix from obtaining the maximum packing and due to the presence of larger microporosity, it can produce voids and thus raise the void content as explained in section 3.1. This finding is in agreement with Quercia et al. [31], showing the powder olivine silica has a limited strength increase for cement-based materials. When the curing age is prolonged to 3 days, the strength of C-OnS and C-nS increases to 122.6 and 120.8 MPa, respectively. However, the reference group still obtains a lower strength of 112.2 MPa. As the curing time further increases to 7 days, the strength of plain UHPC increases to 132.6 MPa. The silicas groups still have a higher strength, reaching 143.6 MPa for C-OnS and 138.6 MPa for C-nS. At 28 days, the strength of all the four groups reach above 150 MPa. Nevertheless, the gap among colloidal groups narrowed as the strength for C-OnS and C-nS reach 162.5 MPa and 166.3 MPa, respectively.

While both colloidal silicas can enhance compressive strength by substituting cement, the C-OnS contributes to a higher strength than C-nS at the early age. It is attributed to the stronger pozzolanic reactivity of olivine nano silica, as can be observed from the TG and NMR analysis. During the first 7 days, the C–S–H formed from secondary hydration of cement is much higher than C-nS group. The chain length of C–S–H is also longer, and polymerization degree is higher for C-OnS as indicated by NMR analysis. Therefore, combined with the microstructural analysis of the C-OnS group, it can explain the results of compressive strength. While for C-nS, it facilitates both the filler effect and the pozzolanic effect. This can be indicated by the ^{29}Si and ^{27}Al NMR analysis of the C-nS group and the MIP results at 7 days. The Al substitution of Si is higher for C-nS group while the optimization of pores are also more obvious than C-OnS after 7 days. Therefore, the strength from 7 days to 28 days of O-nS group becomes higher than C-OnS groups. That's the reason why the C-nS has a slightly higher compressive strength than C-OnS at later ages.

3.7. Discussion

In this study, a novel and sustainable colloidal nano silica from olivine (C-OnS) is produced and its influence on UHPC performance is investigated and compared to commercial sol-gel colloidal silica (C-nS) and shows promising results. Table 8 shows a summary of different types of nano silica regarding the properties and their dominant effect on the cement hydration at early ages.

As discussed in the study by Lee et al. [13], the seeding effect and pozzolanic reaction of silica fume are relatively less apparent during the first 4 days. Therefore, silica fume used in ultralow w/b ratio systems has a limited influence on cement hydration at early ages unless 80-degree curing is applied. This is due to the low silanol content and surface area, which is the lowest among the four mentioned silicas in Table 8. However, the filler effect is obvious for the silica fume at early ages and pozzolanic effect at later ages, but at a slow reaction rate.

Another type of nano silica used in UHPC is the pyrogenic silica [54]. This production process features a lower silanol content of silica to 1–3 OH/nm^2 [54]. As discussed in the investigation by Oertel et al. [14], the pyrogenic silica enhances early age strength and accelerates hydration, dissolution of alite and formation of C–S–H phases. No noticeable dissolution of silica in the pore solution is detected in pastes containing pyrogenic silica. Also, it increases the surface area for nucleation of C–S–H phases. Therefore, it is found the pyrogenic silica can enhance the early age cement hydration and the filler or nano-seeding effect is dominant.

The commercial colloidal silica made from sol-gel technology shows a much higher pozzolanic reactivity at early ages than the pyrogenic silica and silica fume, according to the results in this study. This is attributed to the higher silanol content of silica due to the sol-gel method, which excludes the high temperature process and produce in a wet route. However, the seeding effect seems not obvious for C-nS compared to pyrogenic silica and silica fume. It shows a very limited acceleration on cement hydration, as presented by the calorimeter test. The strength development is also not obvious at the first 7 days.

However, the olivine colloidal silica obtains the highest silanol content and is much higher than C-nS, pyrogenic silica and silica fume. This special production route excludes high temperature sintering and is precipitated below the isoelectric point of silica (pH less than 2) [55]. The olivine silica contains Q^2, Q^3 and Q^4 silicate species, indicating quite different properties compared to the three kinds of silica mentioned above. Its pozzolanic reactivity is the highest among all types of nano silica, while no obvious seeding effect can be found. Most of the olivine silica is consumed during the first 3 days of curing. Therefore, it can enhance the early age performance of UHPC, however, the refinement of the pore structure is weaker than that of C-nS. Thus, the later age performance still needs further investigations.

4. Conclusions

This study investigates a novel colloidal nano-silica preparation from olivine (C-OnS), which is highly dispersed and low-cost compared to commercial colloidal silica and shows a higher acceleration effect on cement hydration in UHPC at early age. The establishment of using colloidal mill to deagglomerate secondary particles open up possibility to apply on other SCMs. The prepared C-OnS has a positive effect on flowability of UHPC and the reduction of superplasticizer usage. The overall influences of the developed colloidal silica on the performance and microstructure of UHPC are investigated. Based on the results of the study, the following conclusions can be drawn:

1. Colloidal silica is successfully synthesized by using a colloidal mill to deagglomerate the secondary particles of the nano-silica from olivine. The stable suspension of silica nanoparticles can be achieved by adjusting the pH to 9 and adding 0.1% non-ionic surfactant Tween 60, reaching a high zeta potential of −36.0 mV. The particle size distribution of the C-OnS is centered at 164 nm measured by laser light scattering.
2. C-OnS has a better dispersibility in cement paste and UHPC paste compared to olivine silica in powder form. The plastic viscosity is only 1.4 Pa•s for C-OnS 2% UHPC paste while for olivine silica powder, the plastic viscosity increases to 1.7 Pa•s. Therefore, using C-OnS can have a reduction on the use of SP in the UHPC production if the same workability is expected to be achieved. However,

Table 8
Comparison of different kinds of nano-silica and their dominant effects on UHPC at early age.

Types of silica	Surface area (m^2/g)	Particle shape	Silanol content (OH/nm^2)	Particle size (nm)	Pozzolanic effect	Filler effect	Literature
C-OnS	200–400	Irregular spheres	8–15	10–20	Strong	Weak	This study
C-nS (sol-gel)	20–50	Round spheres	4–5	50–100	Medium	Medium	This study
Pyrogenic silica	50–100	Round spheres	1–3	73–291	Weak	Strong	[14]
Silica fume	15–30	Round spheres	< 1	200–400	Weak	Strong	[13]

compared to C-nS, the effect on plastic viscosity is similar, they both increase the viscosity of plain UHPC paste to a higher extent due to the high surface area.

3. C-OnS can promote the cement hydration better than C-nS at early ages according to the results of calorimeter, thermal gravimetric analysis, and ^{29}Si and ^{27}Al nuclear magnetic resonance. The reason is that C-OnS obtains more silanol content and surface area compared with C-nS. Also, the silicate species of C-OnS include Q^4, Q^3 and Q^2, indicating a better silica solubility in pore solution of UHPC.
4. The mean chain length of C–S–H is longer for C-OnS samples than that of C-nS at early ages as indicated by ^{29}Si NMR. The Al (IV) species replace the Si in C–S–H forming C-(A)-S-H due to the formation of secondary hydration products C–S–H (α) by consuming Ca$(OH)_2$. This phenomenon happens at first 3 days for C-OnS while takes place more intense at 7 days for C-nS.
5. The gel pore volume of UHPC with 2% C-OnS is higher than that of C-nS and REF at 1 and 7 days, indicating more C–S–H (α) is produced due to quick pozzolanic reaction. The nitrogen sorption and MIP result shows the C-nS can better facilitate filler effect in UHPC paste, thus reducing the small capillary pore volume better than C-OnS at 7 day.
6. The ultrahigh performance concrete obtains a higher early age strength with the incorporation of C-OnS and C-nS. The early age strength from 1 day to 7 days is higher for C-OnS group. While the 28 days strength of UHPC is almost the same for C-OnS and C-nS but still higher than REF. Therefore, the C-OnS mainly increases the first 7 days strength of UHPC.

Declaration of competing interest

The authors declare that they have no known competing financial interests or personal relationships that could have appeared to influence the work reported in this paper.

Acknowledgement

This research is funded by National Natural Science Foundation of China (Grant No. 52178246), China Scholarship Council (CSC) Fund (Grant No. 201706950053) and Eindhoven University of Technology. Eurosupport (the Netherlands) and ENCI (the Netherlands) are thanked for providing materials. Shaojie Li MSc. is acknowledged for the experimental support on ^{29}Si and ^{27}Al NMR test.

Appendix A. Supplementary data

Supplementary data to this article can be found online at https://doi.org/10.1016/j.cemconcomp.2022.104564.

References

[1] H. Van Damme, H. Van Damme, Concrete material science : past , present , and future innovations, Cement Concr. Res. 112 (2018) 5–24, https://doi.org/10.1016/j.cemconres.2018.05.002.
[2] E. Fehling, M. Schmidt, J. Walraven, T. Leutbecher, S. Fröhlich, Ultra-High Performance Concrete UHPC: Fundamentals, Design, Examples, 2015, https://doi.org/10.1002/9783433604076.
[3] R. Jing, Y. Liu, P. Yan, Uncovering the effect of fly ash cenospheres on the macroscopic properties and microstructure of ultra high-performance concrete (UHPC), Construct. Build. Mater. 286 (2021), 122977, https://doi.org/10.1016/j.conbuildmat.2021.122977.
[4] Z. Mo, R. Wang, X. Gao, Hydration and mechanical properties of UHPC matrix containing limestone and different levels of metakaolin, Construct. Build. Mater. 256 (2020), 119454, https://doi.org/10.1016/j.conbuildmat.2020.119454.
[5] Ç. Yalçınkaya, O. Çopuroğlu, Hydration heat, strength and microstructure characteristics of UHPC containing blast furnace slag, J. Build. Eng. 34 (2021), https://doi.org/10.1016/j.jobe.2020.101915.
[6] Y. Ma, J. Bai, C. Shi, S. Sha, B. Zhou, Effect of PCEs with different structures on hydration and properties of cementitious materials with low water-to-binder ratio, Cement Concr. Res. 142 (2021), 106343, https://doi.org/10.1016/j.cemconres.2020.106343.
[7] L. Wang, N. Ur Rehman, I. Curosu, Z. Zhu, M.A.B. Beigh, M. Liebscher, L. Chen, D. C.W. Tsang, S. Hempel, V. Mechtcherine, On the use of limestone calcined clay cement (LC3) in high-strength strain-hardening cement-based composites (HS-SHCC), Cement Concr. Res. 144 (2021), 106421, https://doi.org/10.1016/j.cemconres.2021.106421.
[8] R. Yu, P. Spiesz, H.J.H. Brouwers, Effect of nano-silica on the hydration and microstructure development of Ultra-High Performance Concrete (UHPC) with a low binder amount, Construct. Build. Mater. 65 (2014) 140–150.
[9] M. Aly, M.S.J. Hashmi, A.G. Olabi, M. Messeiry, E.F. Abadir, A.I. Hussain, Effect of colloidal nano-silica on the mechanical and physical behaviour of waste-glass cement mortar, Mater. Des. 33 (2012) 127–135, https://doi.org/10.1016/j.matdes.2011.07.008.
[10] M. Azimi-Pour, H. Eskandari-Naddaf, Synergistic effect of colloidal nano and micro-silica on the microstructure and mechanical properties of mortar using full factorial design, Construct. Build. Mater. (2020), https://doi.org/10.1016/j.conbuildmat.2020.120497.
[11] B. Bose, C.R. Davis, K.A. Erk, Microstructural refinement of cement paste internally cured by polyacrylamide composite hydrogel particles containing silica fume and nanosilica, Cement Concr. Res. 143 (2021).
[12] F. Kontoleontos, P.E. Tsakiridis, A. Marinos, V. Kaloidas, M. Katsioti, Influence of colloidal nanosilica on ultrafine cement hydration: physicochemical and microstructural characterization, Construct. Build. Mater. 35 (2012) 347–360, https://doi.org/10.1016/j.conbuildmat.2012.04.022.
[13] N.K. Lee, K.T. Koh, M.O. Kim, G.S. Ryu, Uncovering the role of micro silica in hydration of ultra-high performance concrete (UHPC), Cement Concr. Res. 104 (2018) 68–79.
[14] T. Oertel, U. Helbig, F. Hutter, H. Kletti, G. Sextl, Influence of amorphous silica on the hydration in ultra-high performance concrete, Cement Concr. Res. 58 (2014) 121–130, https://doi.org/10.1016/j.cemconres.2014.01.006.
[15] G. Quercia, G. Hüsken, H.J.H. Brouwers, Water demand of amorphous nano silica and its impact on the workability of cement paste, Cement Concr. Res. 42 (2012) 344–357, https://doi.org/10.1016/j.cemconres.2011.10.008.
[16] Z. Wu, K.H. Khayat, C. Shi, Effect of nano-SiO2 particles and curing time on development of fiber-matrix bond properties and microstructure of ultra-high strength concrete, Cement Concr. Res. 95 (2017) 247–256.
[17] N.M. Azmee, N. Shafiq, Ultra-high performance concrete: from fundamental to applications, Case Stud. Constr. Mater. 9 (2018), https://doi.org/10.1016/j.cscm.2018.e00197.
[18] Y. Sargam, K. Wang, A. Tsyrenova, S. Jiang, F. Liu, Effects of anionic and nonionic surfactants on the dispersion and stability of nanoSiO2 in aqueous and cement pore solutions, Cement Concr. Res. v1 (2020), 106417, https://doi.org/10.1016/j.cemconres.2021.106417.
[19] A. Vandenberg, H. Bessaies-Bey, K. Wille, N. Roussel, Influence of mixing on the generation of nanoparticles in cement systems, Cement Concr. Res. 143 (2021), 106379, https://doi.org/10.1016/j.cemconres.2021.106379.
[20] N. Ye, J. Zheng, X. Ye, J. Xue, D. Han, H. Xu, Z. Wang, L. Zhang, Performance enhancement of rubber composites using VOC-Free interfacial silica coupling agent, Compos. B Eng. 202 (2020), 108301, https://doi.org/10.1016/j.compositesb.2020.108301.
[21] X. Wu, J. Zheng, B. Han, L. Zhang, J. Lu, X. Ye, Designing novel epoxy-terminated polybutadiene to construct chemical interface between nanosilica and rubbers with green nature, Compos. B Eng. 178 (2019) 107451, https://doi.org/10.1016/j.compositesb.2019.107451.
[22] K. Kolman, O. Nechyporchuk, M. Persson, K. Holmberg, R. Bordes, Combined nanocellulose/nanosilica approach for multiscale consolidation of painting canvases, ACS Appl. Nano Mater. 1 (2018) 2036–2040, https://doi.org/10.1021/acsanm.8b00262.
[23] S. Kongparakul, S. Kornprasert, P. Suriya, D. Le, C. Samart, N. Chantarasiri, P. Prasassarakich, G. Guan, Self-healing hybrid nanocomposite anticorrosive coating from epoxy/modified nanosilica/perfluorooctyl triethoxysilane, Prog. Org. Coating 104 (2017) 173–179, https://doi.org/10.1016/j.porgcoat.2016.12.020.
[24] Z. Asadi, R. Norouzbeigi, Synthesis of colloidal nanosilica from waste glass powder as a low cost precursor, Ceram. Int. 44 (2018) 22692–22697, https://doi.org/10.1016/j.ceramint.2018.09.050.
[25] A. Lazaro, N. Vilanova, L.D. Barreto Torres, G. Resoort, I.K. Voets, H.J.H. Brouwers, Synthesis, polymerization, and assembly of nanosilica particles below the isoelectric point, Langmuir 33 (2017) 14618–14626, https://doi.org/10.1021/acs.langmuir.7b01498.
[26] E.D.E.R. Hyde, A. Seyfaee, F. Neville, R. Moreno-Atanasio, Colloidal silica particle synthesis and future industrial manufacturing pathways: a review, Ind. Eng. Chem. Res. 55 (2016) 8891–8913, https://doi.org/10.1021/acs.iecr.6b01839.
[27] K. Tadanaga, K. Morita, K. Mori, M. Tatsumisago, Synthesis of monodispersed silica nanoparticles with high concentration by the Stöber process, J. Sol. Gel Sci. Technol. 68 (2013) 341–345, https://doi.org/10.1007/s10971-013-3175-6.
[28] A. Lazaro, H.J.H. Brouwers, G. Quercia, J.W. Geus, The properties of amorphous nano-silica synthesized by the dissolution of olivine, Chem. Eng. J. 211–212 (2012) 112–121, https://doi.org/10.1016/j.cej.2012.09.042.
[29] A. Lazaro, M.C. Van De Griend, H.J.H. Brouwers, J.W. Geus, The influence of process conditions and Ostwald ripening on the specific surface area of olivine nano-silica, Microporous Mesoporous Mater. 181 (2013) 254–261, https://doi.org/10.1016/j.micromeso.2013.08.006.
[30] D. Schuiling, Roelof, A Method for Neutralizing Waste Sulfuric Acid by Adding a Silicate, WO/1986/000288, 1986.
[31] G. Quercia, A. Lazaro, J.W. Geus, H.J.H. Brouwers, Characterization of morphology and texture of several amorphous nano-silica particles used in concrete, Cement

Concr. Compos. 44 (2013) 77–92, https://doi.org/10.1016/j.cemconcomp.2013.05.006.
[32] A. Lazaro, G. Quercia, H.J.H. Brouwers, J.W. Geus, Synthesis of a green nano-silica material using beneficiated waste dunites and its application in concrete, World J. Nano Sci. Eng. (2013) 41–51, https://doi.org/10.4236/wjnse.2013.33006, 03.
[33] A. Lazaro, K. Sato, H.J.H. Brouwers, J.W. Geus, Pore structure development of silica particles below the isoelectric point, Microporous Mesoporous Mater. 267 (2018) 257–264, https://doi.org/10.1016/j.micromeso.2018.03.031.
[34] H. Van Damme, Concrete material science: past, present, and future innovations, Cement Concr. Res. 112 (2018) 5–24, https://doi.org/10.1016/j.cemconres.2018.05.002.
[35] T. Ogi, R. Zulhijah, T. Iwaki, K. Okuyama, Recent progress in nanoparticle dispersion using bead mill, KONA Powder Part. J. 2017 (2017) 3–23, https://doi.org/10.14356/kona.2017004.
[36] M. Inkyo, T. Tahara, T. Iwaki, F. Iskandar, C.J. Hogan, K. Okuyama, Experimental investigation of nanoparticle dispersion by beads milling with centrifugal bead separation, J. Colloid Interface Sci. 304 (2006) 535–540, https://doi.org/10.1016/j.jcis.2006.09.021.
[37] A. Lázaro García, Nano-silica Production at Low Temperatures from the Dissolution of Olivine, PhD Thesis, 2014.
[38] R. Yang, R. Yu, Z. Shui, C. Guo, S. Wu, X. Gao, S. Peng, The physical and chemical impact of manufactured sand as a partial replacement material in Ultra-High Performance Concrete (UHPC), Cement Concr. Compos. 99 (2019) 203–213.
[39] X. Wang, R. Yu, Z. Shui, Q. Song, Z. Liu, Z. Liu, S. Wu, Optimized treatment of recycled construction and demolition waste in developing sustainable ultra-high performance concrete, J. Clean. Prod. 221 (2019) 805–816.
[40] A.H.M. Andreasen, Über die Beziehung zwischen Kornabstufung und Zwischenraum in Produkten aus losen Körnern (mit einigen Experimenten), Kolloid Z. 50 (1930) 217–228.
[41] R. Yu, P. Spiesz, H.J.H. Brouwers, Mix design and properties assessment of ultra-high performance fibre reinforced concrete (UHPFRC), Cement Concr. Res. 56 (2014) 29–39.
[42] G. Hüsken, A Multifunctional Design Approach for Sustainable Concrete: with Application to Concrete Mass Products, 2010.
[43] R. Yu, P. Spiesz, H.J.H. Brouwers, Development of ultra-high performance fibre reinforced concrete (UHPFRC): towards an efficient utilization of binders and fibres, Construct. Build. Mater. 79 (2015) 273–282.
[44] X. Wang, R. Yu, Q. Song, Z. Shui, Z. Liu, S. Wu, D. Hou, Optimized design of ultra-high performance concrete (UHPC) with a high wet packing density, Cement Concr. Res. 126 (2019), 105921, https://doi.org/10.1016/j.cemconres.2019.105921.
[45] A. Mendes, W.P. Gates, J.G. Sanjayan, F. Collins, NMR, XRD, IR and synchrotron NEXAFS spectroscopic studies of OPC and OPC/slag cement paste hydrates, Mater. Struct. Constr. 44 (2011) 1773–1791, https://doi.org/10.1617/s11527-011-9737-6.
[46] B. Walkley, J.L. Provis, Solid-state nuclear magnetic resonance spectroscopy of cements, Mater. Today Adv. 1 (2019), 100007, https://doi.org/10.1016/j.mtadv.2019.100007.
[47] K. Johansson, C. Larsson, O.N. Antzutkin, W. Forsling, H.R. Kota, V. Ronin, Kinetics of the hydration reactions in the cement paste with mechanochemically modified cement29Si magic-angle-spinning NMR study, Cement Concr. Res. 29 (1999) 1575–1581, https://doi.org/10.1016/S0008-8846(99)00135-0.
[48] L.T. Zhuravlev, V.V. Potapov, Density of silanol groups on the surface of silica precipitated from a hydrothermal solution, Russ. J. Phys. Chem. A. 80 (2006) 1119–1128, https://doi.org/10.1134/S0036024406070211.
[49] M.D. Andersen, H.J. Jakobsen, J. Skibsted, Characterization of white Portland cement hydration and the C-S-H structure in the presence of sodium aluminate by 27Al and 29Si MAS NMR spectroscopy, Cement Concr. Res. 34 (2004) 857–868, https://doi.org/10.1016/j.cemconres.2003.10.009.
[50] A.S. Brykov, A.S. Vasil'Ev, M.V. Mokeev, Hydration of Portland cement in the presence of high activity aluminum hydroxides, Russ. J. Appl. Chem. 85 (2012) 1793–1799, https://doi.org/10.1134/S1070427212120014.
[51] M.R. Jones, D.E. Macphee, J.A. Chudek, G. Hunter, R. Lannegrand, R. Talero, S. N. Scrimgeour, Studies using 27Al MAS NMR of AFm and AFt phases and the formation of Friedel's salt Cem, Concr. Res. 33 (2003) 177–182, https://doi.org/10.1016/S0008-8846(02)00901-8.
[52] T. Isobe, T. Watanabe, J.B. D'Espinose De La Caillerie, A.P. Legrand, D. Massiot, Solid-state 1H and 27Al NMR studies of amorphous aluminum hydroxides, J. Colloid Interface Sci. 261 (2003) 320–324, https://doi.org/10.1016/S0021-9797(03)00144-9.
[53] ASTMC1856, Standard Practice for Fabricating and Testing Specimens of Ultra-high Performance Concrete, 2017.
[54] A. Spyrogianni, I.K. Herrmann, K. Keevend, S.E. Pratsinis, K. Wegner, The silanol content and in vitro cytolytic activity of flame-made silica, J. Colloid Interface Sci. 507 (2017) 95–106, https://doi.org/10.1016/j.jcis.2017.07.096.
[55] A. Lazaro, N. Vilanova, L.D.B. Torres, G. Resoort, I.K. Voets, H.J.H. Brouwers, Synthesis, polymerization, and assembly of nanosilica particles below the isoelectric point, Langmuir 33 (2017) 14618–14626, https://doi.org/10.1021/acs.lagmuir.7b01498.